AGU PUBLICATIONS

Paleoceanography

RESEARCH ARTICLE
10.1002/2017PA003133

Key Points:
- Reoccurring nutrient leakage from northern-sourced waters to equatorial Pacific subthermocline waters during peak glacials
- Diminished Southern Ocean Intermediate Water nutrient influence on equatorial Pacific subthermocline during peak glacials
- High-latitude water source switches to the equatorial Pacific during terminations

Supporting Information:
- Supporting Information S1
- Data Set S1
- Data Set S2

Correspondence to:
N. Rippert,
nadine.rippert@gmail.com

Citation:
Rippert, N., Max, L., Mackensen, A., Cacho, I., Povea, P., & Tiedemann, R. (2017). Alternating influence of northern versus southern-sourced water masses on the equatorial Pacific subthermocline during the past 240 ka. *Paleoceanography*, *32*, 1256–1274. https://doi.org/10.1002/2017PA003133

Received 15 APR 2017
Accepted 25 OCT 2017
Accepted article online 28 OCT 2017
Published online 18 NOV 2017

Alternating Influence of Northern Versus Southern-Sourced Water Masses on the Equatorial Pacific Subthermocline During the Past 240 ka

Nadine Rippert[1], Lars Max[1], Andreas Mackensen[1], Isabel Cacho[2], Patricia Povea[2], and Ralf Tiedemann[1]

[1]Alfred-Wegener-Institut Helmholtz Zentrum für Polar- und Meeresforschung, Bremerhaven, Germany, [2]Grup de Recerca Consolidat en Geociències Marines, Departament de Dinàmica de la Terra i de l'Oceà, Universitat de Barcelona, Barcelona, Spain

Abstract The eastern equatorial Pacific (EEP) is a key area to understand past oceanic processes that control atmospheric CO_2 concentrations. Many studies argue for higher nutrient concentrations by enhanced nutrient transfer via Southern Ocean Intermediate Water (SOIW) to the low-latitude Pacific during glacials. Recent studies, however, argue against SOIW as the primary nutrient source, at least during early Marine Isotope Stage 2 (MIS 2), as proxy data indicate that nutrients are better utilized in the Southern Ocean under glacial conditions. New results from the subarctic Pacific suggest that enhanced convection of nutrient-rich Glacial North Pacific Intermediate Water (GNPIW) contributes to changes in nutrient concentrations in equatorial subthermocline water masses during MIS 2. However, the interplay between SOIW versus GNPIW and its influence on the nutrient distribution in the EEP spanning more than one glacial cycle are still not understood. We present a carbon isotope ($\delta^{13}C$) record of subthermocline waters derived from deep-dwelling planktonic foraminifera *Globorotaloides hexagonus* in the EEP, which is compared with published $\delta^{13}C$ records around the Pacific. Results indicate enhanced influence of GNPIW during MIS 6 and MIS 2 compared to today with largest contributions of northern-sourced intermediate waters during glacial maxima. These observations suggest a mechanistic link between relative contributions of northern and southern intermediate waters and past EEP nutrient concentrations. A switch from increased GNPIW (decreased SOIW) to diminished GNPIW (enhanced SOIW) influence on equatorial subthermocline waters is recognized during glacial terminations and marks changes to modern-like conditions in nutrient concentrations and biological productivity in the EEP.

1. Introduction

The modern eastern equatorial Pacific (EEP) acts as the most important source for marine carbon dioxide (CO_2) to the atmosphere (Takahashi et al., 2009). The elevated pCO_2 has been attributed to the upwelling of nutrient-rich waters in combination with low productivity by siliceous phytoplankton that sequesters CO_2 during photosynthesis (Dugdale & Wilkerson, 1998). However, primary productivity of these organisms is currently hindered by low availability of silicic acid ($Si(OH)_4$) and iron in the EEP (Broecker & Peng, 1982; Dugdale et al., 2002; Ryan et al., 2006; Sarmiento et al., 2004), while other macronutrients such as nitrate are not fully utilized and remain high (Robinson et al., 2009). Southern Ocean Intermediate Water (SOIW; after Pena et al., 2013), comprises Subantarctic Mode Water (SAMW) and Antarctic Intermediate Water (AAIW), is the main contributor of Equatorial Pacific Intermediate Water (EqPIW) under modern conditions (Bostock et al., 2010; Goodman et al., 2005; Qu et al., 2009). It only contains depleted $Si(OH)_4$ concentrations relative to other macronutrients, as diatom blooms are very effective in utilizing $Si(OH)_4$ from surface waters in the formation area of SOIW (Hendry & Brzezinski, 2014). This low-$Si(OH)_4$ SOIW is then fed into the low-latitude thermocline (Qu & Lindstrom, 2004). As a result, SOIW contributes about half of the nitrate supply, but only ~30% of the total modern equatorial $Si(OH)_4$ supply into the EEP upwelling system (Dugdale et al., 2002; Sarmiento et al., 2004). Its northern counterpart, the nutrient-elevated (e.g., $Si(OH)_4$) North Pacific Intermediate Water (NPIW), is nowadays mostly bound to about 20°N but extends further south in the western Pacific (Bostock et al., 2010). Therefore, the NPIW reaches the western equatorial Pacific and is transported along the equator, where it accounts for ~70% of the $Si(OH)_4$ supply today (Sarmiento et al., 2004).

Based on silicon isotope records, changes in nutrient utilization indicated that the EEP received three times more $Si(OH)_4$ under glacial conditions, thereby removing the $Si(OH)_4$ limitation within the EEP (Pichevin et al., 2009). Brzezinski et al. (2002) and Matsumoto, Sarmiento, et al. (2002) assumed that excess $Si(OH)_4$ has been delivered via enhanced SOIW to the EEP as described in the Silicic Acid Leakage Hypothesis. This caused diatoms to displace coccolithophores at low latitudes and consequently weakened the carbonate pump and lowered glacial atmospheric pCO_2 (Brzezinski et al., 2002). Stable isotope analysis (Pena et al., 2008), biomarkers (Calvo et al., 2011), planktonic foraminiferal abundances (Yu et al., 2012), neodymium isotope records (ε_{Nd}; Pena et al., 2013), and radiocarbon data (de la Fuente et al., 2015) further argue for an increasing influence of southern-sourced waters on the equatorial thermocline. However, the potential of SOIW in delivering more nutrients to the low-latitude Pacific under glacial conditions is still under debate. Studies found increased glacial productivity in the Southern Ocean, which potentially leaves surface waters rather nutrient depleted and leads to "nutrient-trapping" in the Southern Ocean (Hendry & Brzezinski, 2014; Loubere et al., 2011; Robinson et al., 2014; Rousseau et al., 2016). Furthermore, there is growing debate on the amount of SOIW formed during glacial maxima. An authigenic mineral study found higher oxygen concentrations along the Chilean margin during glacials and correlated these to an increased SOIW production (Muratli et al., 2010). In contrast, a benthic carbon isotope ($\delta^{13}C$) record from the southwest Pacific (Pahnke & Zahn, 2005) and ε_{Nd} values from the tropical Atlantic (Huang et al., 2014; Pahnke et al., 2008) both suggest a reduced production of SOIW during glacial conditions, possibly related to stronger water column stratification. More recently, results from benthic $\delta^{13}C$ records, which form an intermediate to deep water transect at the New Zealand margin, suggest in combination with model results a shoaling of the SOIW/Upper Circumpolar Deep Water (UCDW) boundary during glacials due to an increased freshwater flux into SOIW by melting sea ice (McCave et al., 2008; Ronge et al., 2015).

In the subarctic Pacific, benthic foraminiferal carbon isotope records point to increased formation of Glacial North Pacific Intermediate Water (GNPIW; Duplessy et al., 1988; Keigwin, 1998; Matsumoto, Oba, et al., 2002). In comparison with the modern situation, an ε_{Nd} record proposes a shift in the glacial formation area from mainly the Okhotsk Sea toward the northwest Bering Sea (Horikawa et al., 2010), which was further supported by foraminiferal isotope studies (Knudson & Ravelo, 2015b; Max et al., 2017; Max, Lembke-Jene, et al., 2014; Rella et al., 2012) and reconstructions based on radiolarian assemblages (Matul et al., 2015). Evidence for a strengthened middepth circulation in the North Pacific has been further noticed along the California margin (Stott et al., 2000) and within the eastern tropical North Pacific (ETNP; Leduc et al., 2010). In the equatorial Pacific, benthic carbon isotope signatures show apparent similarities between Bering Sea records and EEP subthermocline waters during glacial boundary conditions, highlighting that the enhanced North Pacific middepth circulation reaches further south during glacial maxima than today (Knudson & Ravelo, 2015b). These similarities and trends in $\delta^{13}C$ signatures further point to an increased nutrient injection from GNPIW into EEP subthermocline waters during Marine Isotope Stage (MIS) 2, which was termed the "North Pacific Nutrient Leakage" (Max et al., 2017).

Recently, there have been several studies that indicate reoccurring signals during the Pleistocene with a shallower penetration of SOIW in the Southern Hemisphere and at the same time higher GNPIW ventilation in the North Pacific (Elmore et al., 2015; Knudson & Ravelo, 2015b; Ronge et al., 2015). However, the interplay between SOIW versus NPIW and its influence on past nutrient distribution in the EEP spanning more than one glacial cycle have not been studied before. Nevertheless, this is important for our understanding of the past oceanic carbon cycle and thought to be intimately linked to past atmospheric CO_2 fluctuations. This study provides new insights into the dynamic interplay of SOIW versus NPIW by comparing $\delta^{13}C$ records from the equatorial subthermocline Pacific, the Pacific sector of the Southern Ocean, and the North Pacific to further disentangle the role of the high-latitude oceans in the nutrient distribution to the equatorial Pacific subthermocline over the past 240 ka.

1.1. Modern Oceanography and Hydrography

The modern EEP is one of the largest high-nitrate–low-chlorophyll areas in the world's oceans (e.g., Dugdale & Wilkerson, 1998; Le Borgne et al., 2002). Delivery of nutrients toward the EEP happens through the eastward flowing equatorial undercurrent (EUC) and the EqPIW. Analyses of cross-equatorial full-depth hydrographic and velocity profiles revealed a complex intermediate depth current system in the equatorial Pacific (Firing et al., 1998). These subthermocline jets include the eastward Southern Intermediate Countercurrent

(~1.5–2.5°S) and the Northern Intermediate Countercurrent (~1.5–3°N) at 500–1,000 m and the westward-directed Southern Equatorial Intermediate Current (~2–4°S), Northern Equatorial Intermediate Current (2–4°N), Equatorial Intermediate Current (~0–2°N), and the Lower Equatorial Intermediate Current (~1°S–1°N; Firing et al., 1998). However, we stick to the definition of Bostock et al. (2010) and use the term EqPIW, as argo float data revealed that these equatorial zonal jets are embedded into a broader system of zonal jets with some of them being highly variable and alternating of small scales and not present all year round (Cravatte et al., 2012; Firing et al., 1998).

The EUC is formed in the western equatorial Pacific by the South Equatorial Current, New Guinea Coastal Undercurrent (NGCUC), and the North Equatorial Counter Current (NECC; Figure 1a; Dugdale et al., 2002; Fine et al., 1994). As the EUC flows eastward across the equatorial Pacific, its upper branch shoals parallel with the thermocline, providing nutrients to the euphotic zone and thereby stimulating primary productivity (Dugdale et al., 2002; Ryan et al., 2006). The lower branch of the EUC does not upwell along the equator, but as it travels across the equator, it receives nutrients from the underlying EqPIW and at the same time provides nutrients to the upper EUC by diapycnal mixing (Dugdale et al., 2002; Qu et al., 2009; Rafter & Sigman, 2015).

In high-nitrate–low-chlorophyll areas including the EEP, primary productivity is stimulated by the input of iron (e.g., Coale et al., 1998; Martin et al., 1994). A variety of iron sources in the formation region of the EUC have been identified to increase the iron concentration within the EUC including hydrothermal venting (Gordon et al., 1997), riverine input, and direct interaction of New Guinea Coastal Undercurrent with continental shelf areas (Mackey et al., 2002) as well as atmospheric dust input along the equator (Winckler et al., 2008). A nutrient analysis by Dugdale et al. (2002) revealed that concentrations of other macronutrients such as nitrate and $Si(OH)_4$ are asymmetrically distributed along the equator but also differ meridionally with both $Si(OH)_4$ and nitrate present in equal proportions north of the equator and low $Si(OH)_4$ to nitrate ratios south of the equator (Table 1; Dugdale et al., 2002). This was further confirmed by geochemical tracer analyses that revealed higher phosphate and silicate concentrations but lower oxygen concentrations in the northern part of the EqPIW (Bostock et al., 2010). As a consequence, the EqPIW was further subdivided into the northern EqPIW and the southern EqPIW (Bostock et al., 2010). The equatorial geochemical signature originates in its source water. Southern EqPIW is formed from mainly SOIW with some influence by diapycnal mixing with upwelling Pacific Deep Water (PDW) under modern conditions (Bostock et al., 2010). Here we use the definition of Pena et al. (2013) with SOIW comprising SAMW and AAIW. SAMW occupies ~300–800 m water depth and is formed in wintertime by vigorous deep mixing along the Subantarctic Front (Bostock et al., 2013; McCartney, 1977). The densest of the circumpolar SAMW is the AAIW, which sinks to 800–1,400 m water depth and is characterized by a prominent salinity minimum (Bostock et al., 2013; McCartney, 1977). PDW formed initially in the North Pacific via upwelling and diffusion of Circumpolar Deep Water (Figure 1; Tomczak & Godfrey, 2005). The deep northern-sourced water mass is the oldest water mass on Earth, characterized by low-oxygen and high-nutrient concentrations with a pronounced silicate maximum as well as elevated CO_2 concentrations (Table 1; Fiedler & Talley, 2006). On the other hand, NPIW, which is the main contributor to Northern EqPIW and NECC (Fine et al., 1994), is never exposed to the surface and does not experience nutrient depletion by biological productivity; hence, nutrient levels remain high (Sarmiento et al., 2004). Instead, modern NPIW formation is tightly coupled to Okhotsk Sea Intermediate Water that is formed in coastal polynyas during wintertime sea-ice formation within the Okhotsk Sea (Shcherbina et al., 2003). The fresh and cold Okhotsk Sea Intermediate Water merges with the northward flowing warm and less dense Kuroshio Current and forms a mixture of these two water masses east of Japan in the northwest Pacific (Talley, 1993). The nutrient-elevated NPIW is found at depths of 300–800 m and spreads south and eastward across the North Pacific and feeds the near-surface flowing California Current as well as North Equatorial Current and NECC (Reid, 1965; Talley, 1993).

In the modern ocean, variations in the spatial gradient of the $\delta^{13}C$ values of the dissolved inorganic carbon (DIC) represent nutrient concentrations and large-scale water mass circulation pattern with high $\delta^{13}C_{DIC}$ values indicating low nutrient concentrations and vice versa (Kroopnick, 1985). The $\delta^{13}C_{DIC}$ of a distinct water mass is altered by in situ accumulation of remineralized particulate organic carbon and mixing with other water masses since isolation from the sea surface. As the water mass flows through the ocean, it accumulates large amounts of sinking and degraded organic material. Consequently, the North Pacific Deep Water records

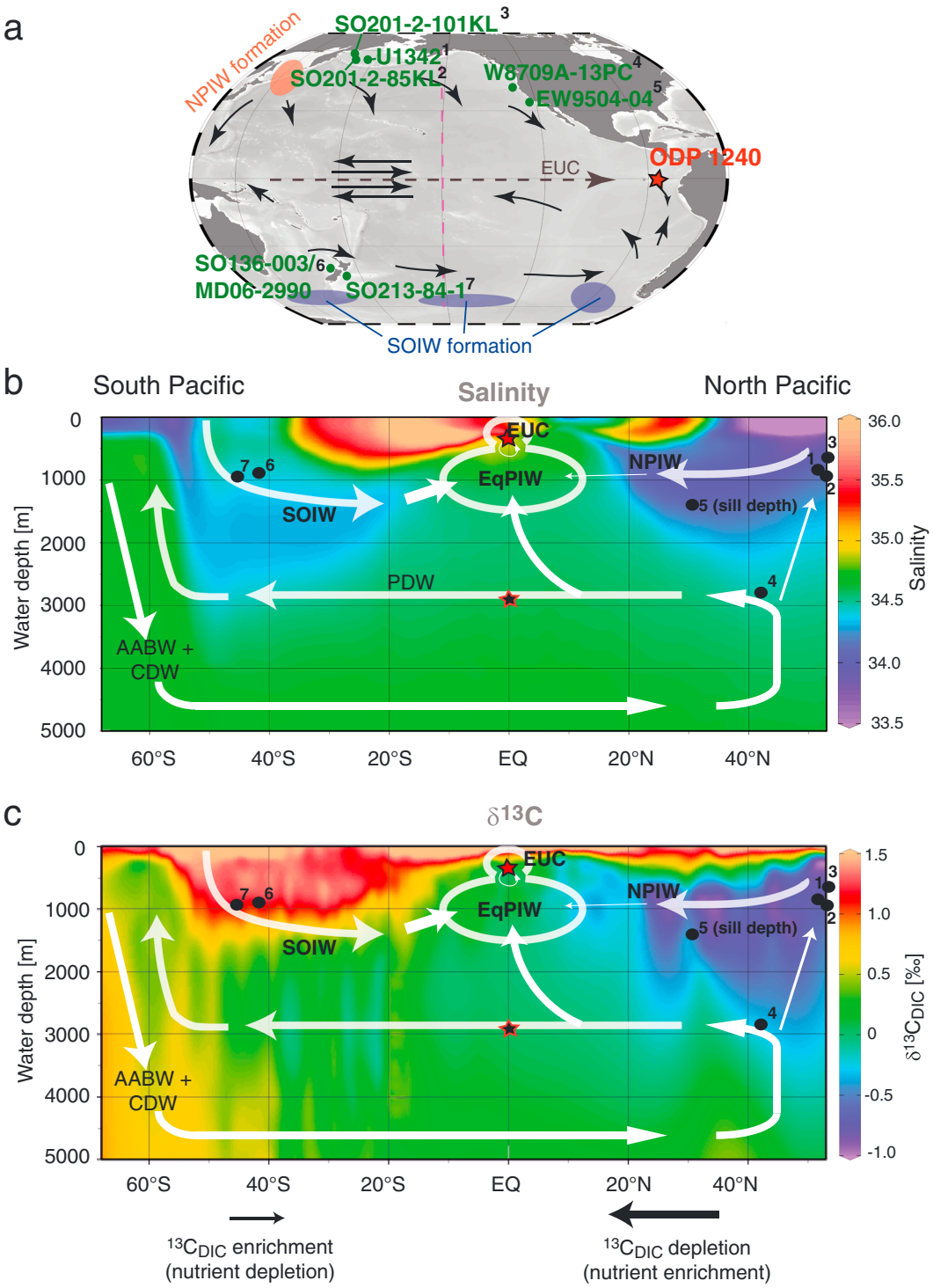

Figure 1. Overview of Pacific Ocean current system and hydrography. (a) Major subsurface currents that are mentioned in the text (after Kessler, 2006; Tchernia, 1980; Tomczak & Godfrey, 2005). Formation areas of North Pacific Intermediate Water (NPIW) and Southern Ocean Intermediate Water (SOIW) are given in colored circles (after Bostock et al., 2013; Talley, 1993). Location of sediment core ODP Site 1240 (this study) is shown with a red star, together with $\delta^{13}C$ reference cores U1342 (1; Knudson and Ravelo, 2015b), SO201-2-85KL (2; Max et al., 2017), SO201-2-101KL (3; Max, Lembke-Jene, et al., 2014), W8709A-13PC (4; Lund & Mix, 1998), EW9504-04 (5; Stott et al., 2000), SO136-003/MD06-2990 (6; Ronge et al., 2015), and SO213-84-1 (7; Ronge et al., 2015). The red line in Figure 1a denotes the transect shown in Figure 1b. (b) Meridional carbon isotope transect across the Pacific Ocean with major middepth to deep water masses (white arrows): Equatorial Pacific Intermediate Water (EqPIW) and equatorial undercurrent (EUC), NPIW and SOIW, PDW = Pacific Deep Water, AABW = Antarctic Bottom Water, and CDW = Circumpolar Deep Water. Red star indicates location of ODP Site 1240 benthic (open) and ODP Site 1240 *G. hexagonus* (full). Black dots denote the reference cores from Figure 1a (assignment through small numbers). Maps and transect were generated using Ocean Data View (Schlitzer, 2015) using data from Schmittner et al. (2013).

Table 1
Modern Geochemical Characteristics for Different Intermediate and Deep Water-Masses at Their Origin

Tracer	NPIW	EUC + EqPIW[a]	SOIW	PDW	AABW
Salinity[b,c]	33.9–34.1	34.5–34.7	34.3–34.5	34.6–34.7	34.6–34.8
Average potential density (σ_θ)[b,d,e]	26.8	26.6–27.0	27.1	27.7–27.8	>27.8
Oxygen (μmol/kg)[e]	0–150	0–80	150–250	100–135	190–210
Nitrate (μmol/kg)[e]	25–45	30–40	20–35	37–40	31–34
Silicate (μmol/kg)[e]	60–150	20–50	5–50	150–170	110–125
Phosphate (μmol/kg)[e]	2.0–3.2	1.9–2.7	1.4–2.3	2.4–2.8	2.1–2.3
$\delta^{13}C$ (‰)[f]	−0.7	0–0.1	1.1	−0.1	0.4

[a]Values determined for 300–500 m water depth. [b]Values from Bostock et al. (2010). [c]Values from Locarnini et al. (2013). [d]Values from Fiedler and Talley (2006). [e]Values from Key et al. (2004). [f]Values from Schmittner et al. (2013).

lowest $\delta^{13}C_{DIC}$ values and highest nutrient concentrations in the world oceans (e.g., Duplessy et al., 1988; Figure 1).

2. Materials and Methods

2.1. Material and Stable Isotope Analyses

We measured stable oxygen ($\delta^{18}O$) and carbon ($\delta^{13}C$) isotopes of deep-dwelling planktonic foraminifera *Globorotaloides hexagonus* and of benthic *Cibicidoides wuellerstorfi* from ODP Site 1240 at the northern flank of Carnegie Ridge in the Panama Basin (0°01.31′N, 86°27.76′W, 2,921 m water depth; Mix et al., 2003; Figure 1, supporting information Tables S1 and S2). For stable isotope analyses, five specimens of *G. hexagonus* (250–315 μm size fraction) and four to five specimens of *C. wuellerstorfi* (>215 μm size fraction) were picked from each sample. The measurements of *G. hexagonus* were conducted on a Thermo Fisher Scientific MAT 253 mass spectrometer coupled to an automatic carbonate preparation device Kiel CARBO IV at Alfred Wegener Institute, Helmholtz Centre for Polar and Marine Research (AWI). Please note that the first 7.9 m of the analyzed $\delta^{13}C_{G.hexagonus}$ values of ODP Site 1240 (spanning about 60 ka) have already been published in Max et al. (2017). Isotope values of *C. wuellerstorfi* were analyzed using a Finnigan MAT 252 mass spectrometer fitted with a Kiel Carbonate Device I in the Scientific and Technological Center of the University of Barcelona (CCiT-UB). Both isotope measurements were calibrated via the international standard NBS 19, and all results are given in δ notation versus Vienna Peedee belemnite. The precision of the measurements at AWI, determined over a 1 year period and based on repeated analysis of an internal laboratory standard (Solnhofen limestone), is ±0.06‰ and ±0.08‰ for carbon and oxygen isotopes, respectively. The external reproducibility at CCiT-UB was always better than ±0.06‰ for $\delta^{18}O$ and ±0.03‰ for $\delta^{13}C$.

To validate the depth habitat of *G. hexagonus*, we determined its apparent calcification depth (ACD) using the uppermost core top sample (at 10 cm; details described in Max et al., 2017). The ACD assessment indicates an ACD of 340–430 m water depth that agrees with studies from the central equatorial Pacific (Rippert et al., 2016) and North Pacific (Ortiz et al., 1996).

We further compiled published benthic $\delta^{18}O$ and $\delta^{13}C$ records from the North Pacific and the Southern Ocean to investigate the variable influence from northern and southern intermediate water masses following the approach of Max et al. (2017). As a northern end-member record, we selected Bering Sea sediment core U1342 from 54.83°N, 176.92°E, and 818 m water depth (Knudson & Ravelo, 2015b). This long sediment core with excellent foraminifera preservation has been shown to trace orbital-scale changes in NPIW (Knudson & Ravelo, 2015b). As a South Pacific end-member, we selected sediment core SO136-003/MD06-2990 (referred to as MD06 in the rest of the paper) from 42.19°S, 169.55°E, and 943 m water depth (Ronge et al., 2015; Figure 1). Ronge et al. (2015) demonstrated by using a $\delta^{13}C$ transect off New Zealand and modeling results that MD06 is exclusively bathed in SOIW, while the often cited $\delta^{13}C$ record of sediment core MD97-2120 (Pahnke & Zahn, 2005) is affected by vertical movements of the SOIW/UCDW boundary (see also McCave et al., 2008).

2.2. Stratigraphic Approach

We improved existing age models of the first 29 meters composite depth (m.c.d.) from ODP Site 1240 (Pena et al., 2008), MD06 (Ronge et al., 2015), and U1342 (Knudson & Ravelo, 2015b) by a combination of published

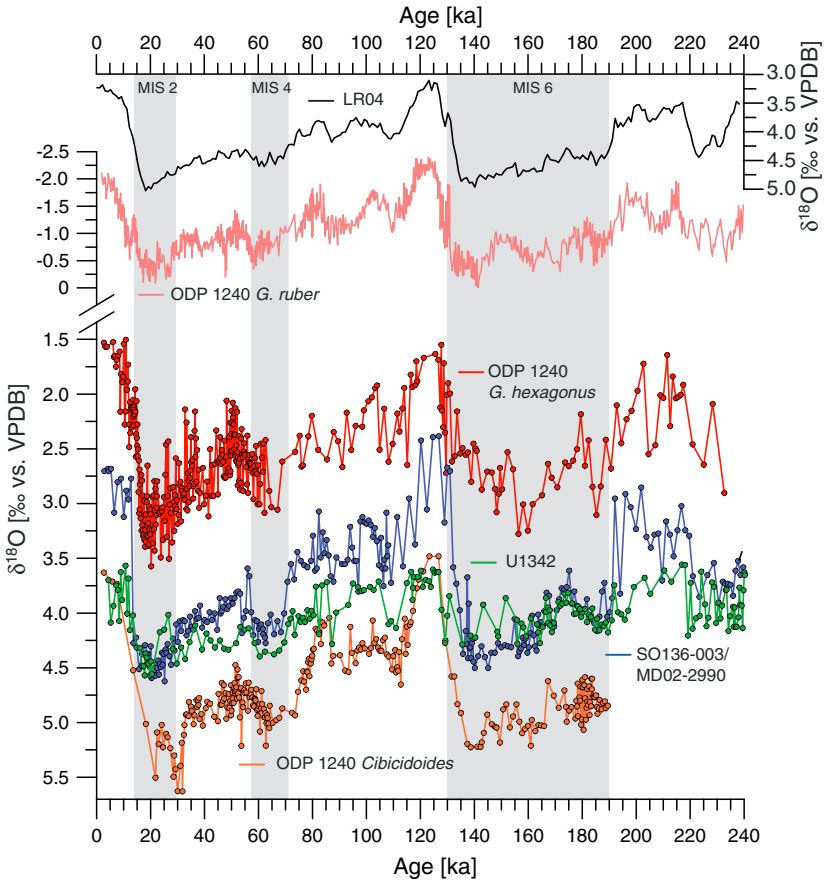

Figure 2. Stratigraphic correlation of published and newly generated $\delta^{18}O$ records with respect to the benthic $\delta^{18}O$ reference stack (LR04, black; Lisiecki & Raymo, 2005). ODP Site 1240 *G. ruber* (light red; Pena et al., 2008), ODP Site 1240 *G. hexagonus* (dark red; this study), SO136-003/MD06-2990 *C. wuellerstorfi* (blue; Ronge et al., 2015), ODP Site 1240 *Cibicidoides* (orange; this study) and U1342 *U. peregrina* (green; Knudson & Ravelo, 2015b). For comparison, all *Cibicidoides* values were corrected to *Uvigerina* using a constant fractionation factor of +0.64.

radiocarbon dating (if available) and $\delta^{18}O$ correlation to the global benthic $\delta^{18}O$ stack LR04 (Lisiecki & Raymo, 2005) using the software AnalySeries 2.0 (Paillard et al., 1996; Figure 2). For the age model of ODP Site 1240, we used the established age model from Pena et al. (2008) for the first 5.2 m.c.d. based on 17 accelerator mass spectrometry ^{14}C dates that cover the first ~38 ka. For the sediment depth interval between 5.2 m.c.d. and ~19 m.c.d., we used our newly generated benthic $\delta^{18}O_{Cibicidoides}$ record of ODP Site 1240 in combination with the $\delta^{18}O$ record of deep-dwelling planktonic foraminifera *G. hexagonus*, which were aligned graphically to the LR04 record (Lisiecki & Raymo, 2005). Beyond the range of the $\delta^{18}O_{Cibicidoides}$ record (~19–29.4 m.c.d.), we took the $\delta^{18}O_{G.hexagonus}$ record and visually tuned it to the LR04 stack. As the *G.hexagonus* record is in only low-resolution during that time interval, we additionally used the surface-dwelling planktonic species *Globigerinoides ruber* record of ODP Site 1240 (Pena et al., 2008) to constrain the developed age model (Figure 2). Furthermore, the ash layer "L" (Ninkovich & Shackleton, 1975) located at 25.71 m.c.d. was considered as well (Pena et al., 2008). Our age model estimation yields an age of the ash layer "L" of 235.83 ka, which is in the range of the previously estimated age of 230 ± 10 ka (Ninkovich & Shackleton, 1975).

For the age model of site MD06, we used the six ^{14}C dates of Ronge et al. (2015) dating back ~25 ka and beyond that graphically tuned the benthic *Cibicidoides wuellerstorfi* $\delta^{18}O$ record to the LR04 record. For U1342 we used the $\delta^{18}O$ values measured on *Uvigerina peregrina* (Knudson & Ravelo, 2015b) and graphically aligned them to LR04.

As a result, the sediment record from 0 to 29.4 m.c.d. of ODP Site 1240 comprises the time interval of the last 300 kyr. The sampling distance provides an average time resolution of 0.23 kyr for the first 60 ka and 1.4 kyr

for 60–240 ka. The upper 9.4 m of sediment core MD06 and the upper 39.4 m of U1342 (core composite depth below seafloor, CCSF-A) cover the time interval of the last 351.7 kyr and 1,260 kyr, with an average temporal resolution of 0.91 kyr and 1.16 kyr, respectively (Figure 2). For the comparison in Figure 2, all $\delta^{18}O_{Cibicidoides}$ values were corrected to *Uvigerina* using a constant fractionation factor of +0.64 according to Shackleton and Opdyke (1973) and Zahn et al. (1986). Supporting Information Table S3 summarizes all age control points used for ODP Site 1240, MD06, and U1342. To have a sufficient resolution for our comparisons, we only take the first 240 ka of the analyzed sediment cores into account.

3. Carbon Isotopes as Proxy for Nutrient Concentrations

Over the past decades, it has been shown that the $\delta^{13}C$ signatures of specific benthic foraminiferal species tests are closely related to the $\delta^{13}C_{DIC}$ signature of ambient seawater. This makes foraminiferal $\delta^{13}C$ a widely applied proxy to trace past changes in circulation and nutrient conditions in the global ocean (Berger et al., 1978; Bostock et al., 2010; Curry & Oppo, 2005; Duplessy et al., 1984, 1988; Keigwin, 1998; Knudson & Ravelo, 2015b; Matsumoto, Oba, et al., 2002; Mix et al., 1991; Oppo & Fairbanks, 1990; Rickaby & Elderfield, 2005; Stott et al., 2000; Zahn et al., 1991).

In this study we compare the epibenthic *C. wuellerstorfi* and infaunal *U. peregrina* with the subthermocline dwelling planktonic species *G. hexagonus*. Differences in species habitat or ecology might affect the $\delta^{13}C$ interpretation. *C. wuellerstorfi* lives epibenthic or elevated above the sediment surface (Lutze & Thiel, 1989), and its calcitic test $\delta^{13}C$ has been shown to reliably record the water $\delta^{13}C_{DIC}$ signal without significant deviation (Duplessy et al., 1984). The influence of seasonal depositions of phytodetritus layers might affect the $\delta^{13}C$ of benthic foraminifera (Mackensen et al., 1993). However, this influence was excluded for MD06 due to negligible glacial–interglacial changes in paleoproductivity (Ronge et al., 2015). In contrast, infaunal *U. peregrina* was found to correlate with accumulation rates of organic carbon, which leads to a disequilibrium from bottom water $\delta^{13}C_{DIC}$ (Zahn et al., 1986). In this study we used the corrected *U. peregrina* values from Knudson and Ravelo (2015b), who converted the $\delta^{13}C_{U.peregrina}$ values to $\delta^{13}C_{C.wuellerstorfi}$ values by using a constant adjustment factor of +0.9‰ (Duplessy et al., 1984). However, this offset was shown to be highly variable ranging from +1.1‰ during the Holocene to +0.1‰ during MIS 2 around New Zealand (Elmore et al., 2015; McCave et al., 2008), and there are some indications that it varied even further north (Carriquiry et al., 2015; Mix et al., 1995). Nevertheless, we assume that an adjusted correction factor would change the amplitude but not the direction of the curve. Given, that there are no studies available from the subarctic Pacific that determine the variable offset between *Cibicidoides* and *Uvigerina*, we refrained from using a variable $\delta^{13}C$ offset factor and used the correction for *U. peregrina* values given by Knudson and Ravelo (2015b). For planktonic *G. hexagonus*, we assume a constant calcification depth over time. Furthermore, we do not correct $\delta^{13}C$ values of *G. hexagonus* for disequilibrium effects as the few available studies infer a minor carbon isotope offset to ambient $\delta^{13}C_{DIC}$ (Birch et al., 2013; Rippert et al., 2016).

Intermediate and deep water-masses from different end-members have a characteristic $\delta^{13}C_{DIC}$ signature (Figure 1, Table 1), depending on the biological cycle and thermodynamically driven gas exchange between the surface ocean and the atmosphere (Lisiecki, 2010; Mackensen et al., 1993; Rohling & Cook, 1999). The latter is particularly important in the source region of intermediate waters; with each 1°C drop in temperature, the $\delta^{13}C_{DIC}$ increases by 0.1‰ (Broecker & Maier-Reimer, 1992; Mackensen, 2012). In the Southern Ocean, the glacial drop in $\delta^{13}C$ of intermediate waters is similar to the $\delta^{13}C$ drop recorded in UCDW; thus, it was assumed that the thermodynamic effect is insignificant (Ronge et al., 2015). In the subarctic Pacific, the modern and glacial formations of intermediate waters are linked to sea-ice formation when surface-ocean temperatures are close to the freezing point (Rella et al., 2012). Given that the formation conditions are nearly congruent, a change in the air-sea gas exchange is assumed to have an only minor effect on the $\delta^{13}C$ signal of the Bering Sea (Max et al., 2017).

Nevertheless, instead of using absolute $\delta^{13}C$ values, we adopted the approach by Knudson and Ravelo (2015b) and used the comparisons between ODP Site 1240 with $U1342_{U.peregrina\ (corr.)}$ (Knudson & Ravelo, 2015b) and MD06 (Ronge et al., 2015) as a proxy for relative nutrient contributions of northern-sourced and southern-sourced waters on the equatorial subthermocline. As a first step to calculate the $\Delta\delta^{13}C$, both

unevenly spaced data sets were put on the same age scale using AnalySeries 2.0 (Paillard et al., 1996). As a next step we calculate the $\Delta\delta^{13}$CNP-EQ$_{G.hex}$ (δ^{13}C at site U1342 minus $\delta^{13}C_{G.hexagonus}$ at ODP Site 1240) as a proxy for assessing GNPIW-nutrient influence and the $\Delta\delta^{13}$CEQ$_{G.hex}$-SP (the $\delta^{13}C_{G.hexagonus}$ at site ODP Site 1240 minus δ^{13}C at MD06) for SOIW-nutrient influence. As a last step we formed the 5 pt moving average. In the modern ocean, U1342 is located in 818 m water depth within the oxygen minimum zone, which is characterized by very low δ^{13}C values (Figure 1). On the other hand, *G. hexagonus* of ODP Site 1240 is situated in ^{13}C enriched (nutrient-depleted) waters that are mainly fed from southern-sourced waters today (Bostock et al., 2010). Consequently, modern $\Delta\delta^{13}$CNP-EQ$_{G.hex}$ values are extremely negative. If the oxygen minimum zone at site U1342 is replaced by well-ventilated GNPIW, the benthic foraminifera would bath in relatively high $\delta^{13}C_{DIC}$ signatures. If GNPIW expands its influence southward into the EEP upwelling system, the equatorial and the subarctic δ^{13}C values would approach each other. A full control of GNPIW on equatorial subsurface water would result in a small but still positive difference ($\Delta\delta^{13}$CNP-EQ$_{G.hex}$), allowing for the aging effect on the δ^{13}C signal. To investigate the SOIW influence, we use the same approach. In the modern ocean, SOIW has relatively high $\delta^{13}C_{DIC}$ values (Figure 1), and the δ^{13}C difference between equatorial subthermocline and SOIW is relatively small. If the injection of SOIW into the EEP upwelling system would cease, we would expect an increased difference in δ^{13}C (large $\Delta\delta^{13}$CEQ$_{G.hex}$-SP).

4. Results

Over the last 240 ka, carbon isotope data from North Pacific core U1342, equatorial subthermocline ODP Site 1240 (*G. hexagonus*), and South Pacific record MD06 oscillate between −0.68‰ and +1.38‰ with high δ^{13}C and thus nutrient-depleted values in the South Pacific and low δ^{13}C (nutrient-elevated) values in the North Pacific (Figure 3). The δ^{13}C amplitude in all three records is similar (0.99–1.14‰) and does not differ significantly. In every record, glacials are characterized by lower δ^{13}C values and interglacials by higher δ^{13}C values displaying the 0.32‰ changes in the terrestrial biosphere and consequently storage in the deep ocean (Gebbie et al., 2015) as well as additional changes in the ocean interior. Equatorial subthermocline δ^{13}C variations are assumed to reflect both nutrient injections and export productivity in the surface ocean of the EEP. Late Holocene equatorial subthermocline values largely follow South Pacific signatures and drift apart from North Pacific values (Figure 3). Contrary, equatorial subthermocline δ^{13}C values show the same temporal evolution as the North Pacific δ^{13}C record during glacial period and become even more pronounced particularly during the glacial maxima MIS 2 and MIS 6.

5. Discussion

By comparing the $\Delta\delta^{13}$C, which is the carbon isotope gradient between water masses of the high latitudes and the EEP subthermocline, we can assess relative changes in the nutrient input into equatorial subthermocline waters. Modern $\Delta\delta^{13}$CEQ$_{G.hex}$-SP values are very negative (−1.0‰). As SOIW largely contributes to equatorial subthermocline waters under modern conditions (Bostock et al., 2010), this might be explained by the larger thermodynamic influence on δ^{13}C in the Southern Ocean compared to the equatorial region (Charles & Fairbanks, 1992; Oppo & Fairbanks, 1989). In addition, δ^{13}C-depleted PDW is also contributing partially to the equatorial subthermocline and thus might explain part of the modern low equatorial δ^{13}C values. Modern $\Delta\delta^{13}$CNP-EQ$_{G.hex}$ values are slightly more positive than $\Delta\delta^{13}$CEQ$_{G.hex}$-SP, although the influence of northern-sourced waters to equatorial subthermocline waters is minor today. However, during the past 240 ka the $\Delta\delta^{13}$C data largely varied (Figure 4). During interstadials, there is a high $\Delta\delta^{13}$C variability, possibly due to the millennial-scale variability of the analyzed sediment cores. During glacials and particularly peak glacial conditions of late MIS 2 (16–19 ka) and late MIS 6 (128–140 ka), the EEP δ^{13}C record largely follows the same absolute values and trends as Bering Sea δ^{13}C values, which indicate that the source water-mass composition and/or contribution reaching the equatorial Pacific differed substantially in the past.

5.1. Reduced SOIW Nutrient Contribution on Equatorial Subthermocline Waters During Glacial Maxima

As a first step, we investigate the relative nutrient contribution of SOIW to equatorial subthermocline waters as the majority of modern equatorial waters are fed by southern-sourced water masses

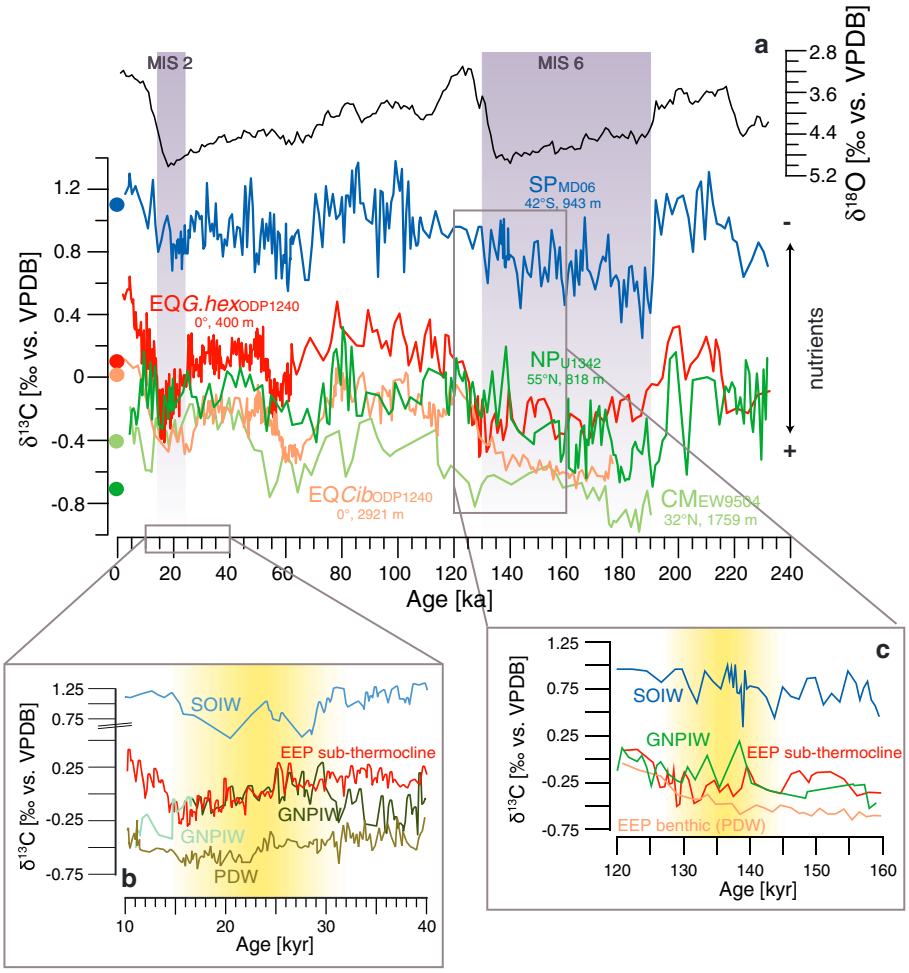

Figure 3. Compilation of Pacific carbon isotope records: (a) Long-term $\delta^{13}C$ records MD06 (South Pacific, SP; blue; Ronge et al., 2015), equatorial ODP Site 1240 *G. hexagonus* (red; this study) and *Cibicidoides* (orange; this study), $U1342_{corr.}$ (North Pacific, NP; dark green; Knudson & Ravelo, 2015b), and EW9504-04 from the California Margin (CM; Stott et al., 2000). Please note that the first 60 ka of the $\delta^{13}C_{G.hexagonus}$ values were previously published in Max et al. (2017). Benthic $\delta^{18}O$ stack (gray; Lisiecki & Raymo, 2005) is shown for stratigraphic orientation. Colored circles denote modern $\delta^{13}C_{DIC}$ at core location. Gray bars mark glacial Marine Isotope Stages (MIS) 2 and 6. (b) High-resolution $\delta^{13}C$ comparison of Max et al. (2017) spanning 10–40 ka BP: Southern Ocean core SO213-84-1 (SOIW, light blue; Ronge et al., 2015), Bering Sea cores SO201-2-101KL (GNPIW, dark green; Max et al., 2017) and SO201-2-85KL (blue-green; Max, Lembke-Jene, et al., 2014), and deep-water record W8709A-13PC (PDW, brown; Lund & Mix, 1998). (c) Detailed records shown in Figure 3a during the end of MIS 6. Yellow shaded bar marks the time of increased GNPIW contribution to EEP subthermocline waters during MIS 2.

(Bostock et al., 2010). Furthermore, higher glacial oxygen concentrations, as suggested by trace element analyses along the Chilean margin, were correlated to an enhanced SOIW formation in the SE Pacific during the last glacial maximum (LGM; Muratli et al., 2010). Our $\delta^{13}C$ difference between the South Pacific and equatorial subthermocline record ($\Delta\delta^{13}CEQ_{G.hex}$-SP) increased from −1.0‰ under modern conditions to −1.2‰ during glacial maxima (Figure 4). This might partially be explained by changes in the SOIW formation conditions within the Southern Ocean as the westerly wind belt moved toward the north during glacial conditions, leading to a change in the wind stress and thereby a change in the air–sea gas exchange of carbon within the formation area of SOIW (Hebbeln et al., 2002). Nevertheless, a drop in temperature would cause increasing $\delta^{13}C$ values (Broecker & Maier-Reimer, 1992), but the $\delta^{13}C_{SP}$ curve shows lighter $\delta^{13}C$ values during the glacials compared to interglacials, which argues for decreasing nutrient concentrations within the southern-sourced water masses. In addition, the SOIW and equatorial subthermocline records show considerably different trends in $\delta^{13}C$ during the glacial. Thus, the increasing $\delta^{13}C$ difference between these records suggests that the nutrient contribution from SOIW into equatorial intermediate waters is reduced during peak glacials.

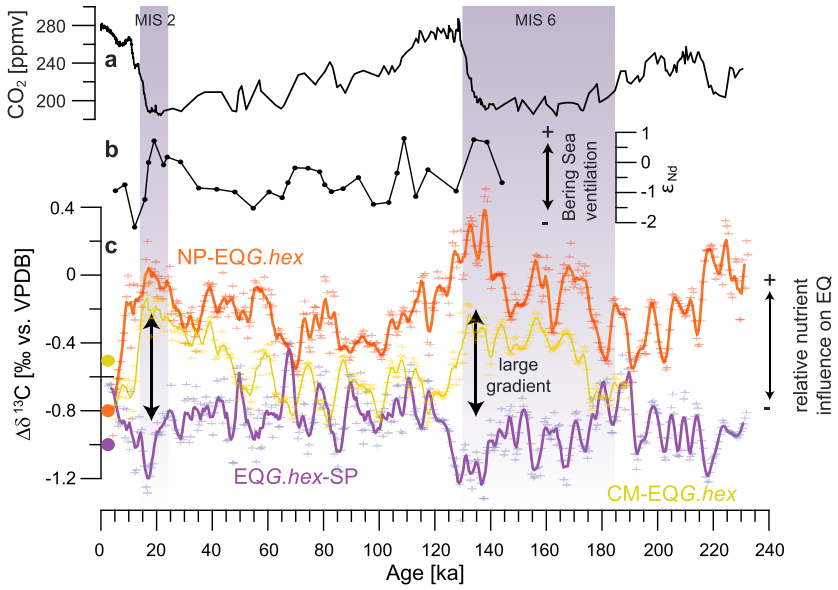

Figure 4. Comparison of different $\delta^{13}C$ records from the Pacific. (a) Atmospheric CO_2 concentrations (Monnin et al., 2001; Pépin et al., 2001; Petit et al., 1999; Raynaud et al., 2005). (b) ε_{Nd} record from Bering Sea core BOW-8A (Horikawa et al., 2010). (c) Data points and 5 pt moving average curves of $\delta^{13}C$ comparison between North Pacific sediment core U1342 (Knudson & Ravelo, 2015b) minus ODP Site 1240 *G. hexagonus* values (this study; red), California Margin record EW9504-04 (Stott et al., 2000) minus ODP Site 1240 *G. hexagonus* values (this study; light green), and ODP Site 1240 *G. hexagonus* values (this study) minus South Pacific record MD06 (Ronge et al., 2015; purple). Colored circles denote $\Delta\delta^{13}C$ values using modern water mass characteristics for the respective comparisons. Gray bars denote glacial Marine Isotope Stages 2 and 6.

The $\delta^{13}C$ values of the penultimate glacial in the South Pacific core are lower than the respective $\delta^{13}C$ values of MIS 2 (Figure 3). A local salinity reconstruction from the central South Pacific estimated contrasting conditions that prevailed in the Southern Ocean between MIS 2 and MIS 6, with water masses saltier than during the Holocene during MIS 6 and contrasting fresher-than-Holocene conditions during MIS 2 (Tapia et al., 2015). To what extent this might influence the nutrient concentration in the Southern Ocean remains elusive as information regarding nutrient (nitrate and silicate) consumption are missing during MIS 6. Nevertheless, we cannot detect a clear difference between the $\Delta\delta^{13}CEQ_{G.hex}$-SP values during MIS 2 and MIS 6 (Figure 4). Instead, both the last peak glacial and the penultimate glacial show an increased difference between equatorial subthermocline waters and SOIW waters compared to modern values. This suggests a reoccurring decreased nutrient contribution from the Southern Ocean toward the equatorial upwelling waters during glacials.

Our analyses point to a reduced southern nutrient-contribution on equatorial subthermocline during peak glacials. This notion is supported by $\delta^{13}C$ studies from New Zealand that propose a shoaling of the SOIW/UCDW boundary from ~2,000 m to ~1,100 m water depth (Elmore et al., 2015; Ronge et al., 2015). This shoaling possibly reflects a reduced production of SOIW due to increased freshwater flux by melting sea ice in the formation area of SOIW (Pahnke & Zahn, 2005; Ronge et al., 2015). Further support for this idea comes from a data compilation in the Southern Ocean that found increased opal accumulation rates in the main formation area of SOIW during the last glacial, which was explained by an increased upwelling due to enhanced wind stress in the Subantarctic Zone and thus a higher supply of nutrients to the euphotic zone (Bradtmiller et al., 2009). Silicon and nitrogen isotope studies from the Subantarctic Zone indicates that the newly available nutrients are almost completely utilized (Hendry & Brzezinski, 2014; Robinson et al., 2014). As a consequence, the amount of silicon exported toward the low latitudes via SOIW must have decreased during MIS 2 as indicated by an isotope mass balance calculation (Beucher et al., 2007). On the other hand, opal flux and productivity reconstructions in the EEP infer greater nutrient concentrations in the equatorial upwelling waters during glacials (e.g., Calvo et al., 2011; Dugdale et al., 2004; Loubere et al., 2003, 2007, 2011). Thus, the largest $\delta^{13}C$ difference between the EEP and Southern Ocean $\delta^{13}C$ values as well as the increased opal accumulation and silicon utilization in the Southern Ocean argues for a relatively reduced contribution of nutrient-depleted southern-sourced waters on equatorial subthermocline during extreme glacials (Figure 5).

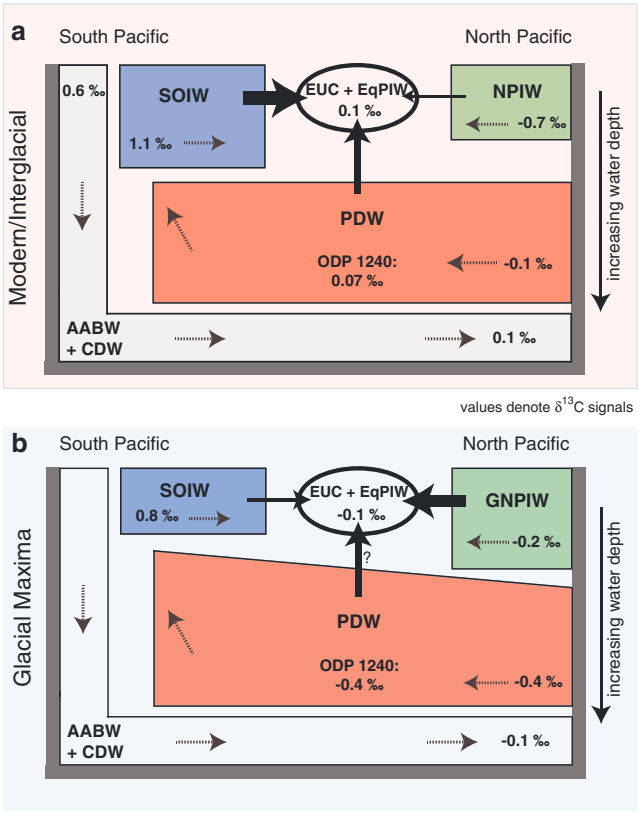

Figure 5. Schematic illustration of changing end-member contributions on EEP upwelling waters during (a) interstadials and (b) glacial maxima. EUC + EqPIW = equatorial undercurrent + Equatorial Pacific Intermediate Water, SOIW = Southern Ocean Intermediate Water, (G)NPIW = (Glacial) North Pacific Intermediate Water, PDW = Pacific Deep Water, AABW + CDW = Antarctic Bottom Water + Circumpolar Deep Water. Black arrows represent possible contributions of end-members, and dashed arrows show current flow. Given values represent $\delta^{13}C$ values that were determined using data from GLODAP (Key et al., 2004), Peterson et al. (2014), and sediment cores analyzed in this study.

5.2. Influence of Northern-Sourced Waters on EqPIW during Peak Glacials

There are two principle water masses sourced from the North Pacific, the PDW and (G)NPIW. The change in equatorial subthermocline values during peak glacials might be explained by an enhanced upwelling of PDW into the equatorial Pacific upwelling system. A comparison of recent ε_{Nd} data between LGM and Holocene values reveals substantially reduced glacial ε_{Nd} values in the EEP, which was explained by a more invigorated deep circulation and higher contribution from deep northern-sourced waters (Hu et al., 2016). Sediment core ODP Site 1240 was retrieved from ~2,900 m water depth, and thus, the benthic $\delta^{13}C$ of ODP Site 1240 reports variability in PDW waters (Figure 1). The comparison between the *G. hexagonus* record and the benthic record of ODP Site 1240 yields an offset of ~0.2‰ during late MIS 2 and MIS 6 (Figure 3). A $\delta^{13}C$ compilation through the Pacific found that the core depth of PDW deepens during the last glacial from ~2,000 m to ~3,000 m water depth (Matsumoto, Oba, et al., 2002). Thus, PDW deepens and might be less well connected to the surface ocean at the equator. In addition, a recent $\delta^{13}C$ comparison between EqPIW and PDW clearly demonstrates that the temporal evolution of PDW was different to EqPIW during MIS 2 with EqPIW $\delta^{13}C$ values increasing steadily, whereas $\delta^{13}C$ values of PDW become further depleted (Figure 3b; Max et al., 2017). This is supported by a study with a carbon-isotope-enabled Earth system model that suggests a reduced deep-ocean ventilation during the LGM (Menviel et al., 2016), which is consistent with recent analyses of radiocarbon activity showing maximal benthic ^{14}C offsets to atmospheric values during the LGM (de la Fuente et al., 2015; Ronge et al., 2016; Skinner et al., 2010, 2015).

We also note that the $\delta^{13}C_{G.hexagonus}$ and $\delta^{13}C_{C.wuellerstorfi}$ values of ODP 1240 approach similar values during the Termination I and II (Figure 3). This "turning point" suggests a pronounced reorganization in the circulation of the Pacific with a possible enhanced contribution from deep water-masses on the equatorial subthermocline. Moreover, during the last glacial termination (at 15 ka), when the determined $\delta^{13}CEQ_{G.hex}$-SP offset decreases (Figure 3), the southward shift of the westerly winds and the Antarctic sea ice together with the strengthened circulation lead to the breakup of the stratification in the Southern Ocean (Menviel et al., 2016; Ronge et al., 2016). As a consequence, it has been argued that the old glacial carbon pool between 2,000 and 4,300 m was eroded and ventilation ages decrease (Ronge et al., 2016). Also within the EEP, a ventilation age reconstruction from ODP Site 1240 estimated that the largest benthic–planktonic ^{14}C offset occurred during peak MIS 2, which decreased to modern values from 15 ka onward (de la Fuente et al., 2015). The combined proxy evidence argue for a similar, or even decreased, glacial PDW exchange with EEP subthermocline waters during peak glacials.

As a next step, we compared the $\delta^{13}C$ subthermocline values to a record from the Bering Sea (U1342) to investigate a possible contribution of GNPIW. Our $\delta^{13}C$ comparison reveals that the difference between Bering Sea and EEP $\delta^{13}C$ values ($\Delta\delta^{13}CNP\text{-}EQ_{G.hex}$) diminishes substantially during glacials, and both $\delta^{13}C$ records approach similar values during late MIS 2 and late MIS 6 (Figure 4). Interestingly, the smallest offset between $\delta^{13}C_{NP}$ and $\delta^{13}CEQ_{G.hex}$ values happen simultaneously to the largest offset between the $\delta^{13}CEQ_{G.hex}$ and $\delta^{13}C_{SP}$ signatures (Figure 4). This might indicate a relatively higher GNPIW contribution to the equatorial upwelling waters than today. Given that GNPIW shows slightly higher $\delta^{13}CEQ_{G.hex}$ values, the $\Delta\delta^{13}CNP\text{-}EQ_{G.hex}$ is slightly positive during glacial maxima. This is in line with a recent high-resolution $\delta^{13}C$ comparison between western Bering Sea (Shirshov Ridge) core SO201-2-101KL and ODP Site 1240 *G. hexagonus* over the past 60 ka that clearly demonstrates the similar absolute $\delta^{13}C$ values and the long-term trend between subthermocline waters and North Pacific waters during early MIS 2 (Figure 3b; Max et al., 2017).

Rella et al. (2012) argue that the formation of GNPIW was initiated in the Bering Sea by the closure of the Bering Strait and an easternmost position of the Aleutian Low. This pooled relatively fresh water within the Bering Sea and fostered a strengthened pycnocline (Riethdorf et al., 2016). The newly formed intermediate water with high oxygen content and low salinities was present in the subarctic Pacific between 700 and 2,600 m water depth from ~60 ka until the beginning of Termination I (Matsumoto, Oba, et al., 2002; Schlung et al., 2013). Further support comes from a ε_{Nd} study indicating that Bering Sea intermediate waters were a principal component of GNPIW during MIS 2 and MIS 6 (Horikawa et al., 2010) and seems to be a reoccurring feature during the past 1.2 Ma (Knudson & Ravelo, 2015b). High nitrogen isotopes indicate an enhanced nutrient utilization in the Bering Sea during MIS 2 and MIS 6 (Brunelle et al., 2010; Galbraith et al., 2008; Knudson & Ravelo, 2015a; Riethdorf et al., 2016). However, it was reported that productivity and export production remained very low during glacial maxima due to an enhanced stratification that prevented upwelling of nutrients from below (Brunelle et al., 2010; Gebhardt et al., 2008; Jaccard et al., 2005; Kienast et al., 2004; Kim et al., 2011; Knudson & Ravelo, 2015a; Riethdorf et al., 2016). A $\delta^{13}C$ comparison during the last 60 ka postulated an increased nutrient injection from GNPIW into EEP subthermocline waters during MIS 2, which was termed the "North Pacific Nutrient Leakage" (Max et al., 2017). With our new data set of a reoccurring decreased $\delta^{13}C$ difference between Bering Sea core and EEP subthermocline, we are now able to show that the "North Pacific Nutrient Leakage" is a recurrent feature that was active not only during the LGM, as has been shown before, but also during the penultimate glacial maximum (MIS 6).

The penultimate glacial maximum (MIS 6) shows even larger $\Delta\delta^{13}$CNP-EQ$_{G.hex}$ values than MIS 2 (Figure 4), which suggests that the "North Pacific Nutrient Leakage" was more enhanced during late MIS 6. A model simulation that investigates the extension of past glaciations found colder MIS 6 conditions with an extensive Eurasian ice sheet compared to MIS 2 (Colleoni et al., 2016). Furthermore, in the Okhotsk Sea, ice-rafted debris accumulation was two to three times higher due to extensive mountain glaciers during MIS 6 compared to the LGM (Nürnberg et al., 2011). Together with the change from seasonal to mobile perennial sea ice cover (Nürnberg et al., 2011), GNPIW formation could have been further intensified during MIS 6. However, not much is known about the circulation in the Okhotsk Sea under penultimate glacial conditions. An expanded GNPIW circulation is supported by an earlier Pacific carbon isotope study that found a relatively larger contribution of well-oxygenated (ventilated) waters between 1,000 and 2,600 m water depth originating in the North Pacific (Duplessy et al., 1988). A more recent stable isotope analyses off the Baja California margin by Herguera et al. (2010) concluded that the observed $\delta^{13}C$-enriched intermediate waters are the result of a changed thermohaline circulation with a possibly enhanced NPIW formation mode. The comparison of $\delta^{13}C$ values of ODP Site 1240 with sediment core EW9504-04 from the Californian margin in the flow path of GNPIW (32°17′N, 118°24′W, 1,759 m water depth, 1,400 sill depth; Figure 1; Stott et al., 2000; $\Delta\delta^{13}$CCM-EQ$_{G.hex}$) yield a similar temporal evolution like $\Delta\delta^{13}C_{NP\text{-}EQG.hex}$, that is, small differences during glacials and high differences during past interglacials (Figure 4). Further south in the ETNP, a carbon isotope study by Leduc et al. (2010) proposed that GNPIW spreads at least till 8°N during the last glacial. Hence, the enhanced ventilated GNPIW seems to have been progressively expanding southward, reaching the California margin and ETNP under glacial conditions, and by the glacial maxima, the volume of GNPIW further expanded as far as the equatorial subthermocline waters (Figure 5). The expansion of relatively nutrient-rich northern-sourced intermediate water should have important implications for the nutrient concentration of the equatorial subthermocline waters, consistent with the findings of Loubere et al. (2003, 2011) and Max et al. (2017). Given the persistent stratification and nearly complete surface nutrient utilization with low organic carbon accumulation that prevailed under glacial conditions in the subarctic Pacific (Riethdorf et al., 2016), the "North Pacific Nutrient Leakage" might have been further enhanced and possibly explains the larger $\Delta\delta^{13}$CNP-EQ$_{G.hex}$ during MIS 6 compared to MIS 2.

The "North Pacific Nutrient Leakage" might have relaxed the nutrient limitation in the EEP. Pichevin et al. (2009) argues that this relaxation in nutrient limitation favored a more efficient biological carbon pump in the EEP and might have contributed to lower atmospheric CO_2 conditions during at least MIS 2. A boron isotope study from the EEP suggests that the EEP turned from a CO_2 source to a CO_2 sink during MIS 2 (Martínez-Botí et al., 2015). Interestingly, times of highest $\Delta\delta^{13}$CNP-EQ$_{G.hex}$ coincide with lowest atmospheric CO_2 concentrations (Figure 4). Whether a reoccurring "North Pacific Nutrient Leakage" might be one of the

triggering mechanisms to lower atmospheric CO_2 concentrations still needs to be investigated with higher resolution cores spanning both MIS 2 and MIS 6.

5.2.1. Possible Mechanisms of an Enhanced GNPIW Extension Into Equatorial Subthermocline

Our $\delta^{13}C$ comparisons together with previously published results show that large-scale reorganization in the formation area of GNPIW and SOIW took place during glacial times and was amplified during glacial maxima. However, glacial/interglacial changes in the western equatorial Pacific also influence the relative high-latitude intermediate-water contribution on the equatorial current system. An idealized layer model shows that the reduction of the Indonesian throughflow during glacial conditions caused an increased contribution of GNPIW to the tropical EqPIW (McCreary & Lu, 2001) and thus reached the EEP subthermocline during glacial maxima. Furthermore, under modern conditions, the NECC, which in turn also feeds the EUC, is fed from both hemispheres (see section 1.1). However, during Northwest Monsoon season, the South Equatorial Current is prevented from injecting into the NECC, and thus, during this season, the NECC is only fed from the north (Tomczak & Godfrey, 2005). A hydrogen isotope record together with regional modeling reconstructed a southward position of the mean Intertropical Convergence Zone and an intensification of northeast trade winds during the last glacial (Pahnke et al., 2007). The glacial southward shift of the Intertropical Convergence Zone is further verified by nitrogen isotope and organic carbon records (Dubois & Kienast, 2011), biomarker analysis (Shaari et al., 2013), and nannofossil assemblages (Staines-Urías et al., 2015). The resulting stronger northeast trades might have reduced the northward penetration and contribution of SOIW to the NECC and possibly also the EqPIW. This provides a possible scenario for our proposed relatively enhanced contribution of northern-sourced waters on the equatorial Pacific subthermocline during late MIS 2 and late MIS 6.

5.3. Deglacial and Interglacial Change in EEP Nutrient Concentration

The $\delta^{13}C$ comparisons between high latitude and EEP upwelling waters yield rapid changes within the Termination I and II. The $\delta^{13}C$ difference between the Bering Sea and ODP Site 1240 increased toward modern values (Figure 4), which suggests decreasing nutrient injections from northern-sourced intermediate waters into EqPIW. It has been shown that a close coupling exists between temperature, sea ice, and GNPIW ventilation (Kim et al., 2011; Rella et al., 2012; Shcherbina et al., 2003). In the Bering Sea, the opening of the Bering Strait due to increasing temperatures and hence sea level rise together with a reduction in sea-ice extent triggered a change in ventilation and productivity (Knudson & Ravelo, 2015b; Riethdorf et al., 2016). Low nitrogen isotopes and higher productivity during warmer periods were explained by a change toward seasonal sea ice, decreased upper-ocean stratification and subsequent enhanced nutrient supply to the euphotic zone by mixing and renewed riverine input (Gebhardt et al., 2008; Knudson & Ravelo, 2015a; Riethdorf et al., 2016). As a result, export production and the deposition of biogenic opal and total organic carbon increased dramatically during the Termination I compared to the last glacial (Kim et al., 2011). In addition, epibenthic $\delta^{13}C$ data from the Bering Sea and the deposition of laminated sediments in the Bering Sea during the Bølling–Allerød and the early Holocene point toward major decreases in middepth oxygenation and hence an expanded oxygen minimum zone that was explained by less well-ventilated intermediate waters (Kuehn et al., 2014; Max, Lembke-Jene, et al., 2014). Interestingly, our $\Delta\delta^{13}C$ comparison further indicates a high variability within interstadials, especially MIS 3 (Figure 4). A $\delta^{13}C$ comparison between the Bering Sea record and the eastern tropical North Pacific by Max et al. (2017) shows a similar long term evolution in $\delta^{13}C$ during MIS 3, however with a higher millennial-scale variability within the eastern tropical North Pacific. Nevertheless, Max et al. (2017) argue for a commencing reorganization of the North Pacific middepth circulation during this time. Unfortunately, the data resolution of the various analyzed sediment cores (except ODP Site 1240) of this study is not sufficient enough to be able to resolve this variability in detail and will be a subject for future research.

There is little information about Termination II from the subarctic Pacific. A temperature and sea-ice reconstruction by Max, Belz, et al. (2014) found ~2°C higher temperatures during the early MIS 5 compared to modern SSTs and the absence of sea ice. As sea ice, temperature, and ventilation are closely connected in the Bering Sea (e.g., Kim et al., 2011), the results of Max, Belz, et al. (2014) point toward a collapse of Bering Sea ventilation also during the penultimate interglacial. Thus, the increasing $\delta^{13}C$ difference reported by our $\delta^{13}C$ comparison between the Bering Sea and the equatorial upwelling waters resemble a similar

pattern of decreased northern-sourced contribution during terminations and interglacials when NPIW was probably more confined to its modern extent.

On the other hand, the $\delta^{13}C$ comparison between the equatorial Pacific and the Southern Ocean ($\Delta\delta^{13}CEQ_{G.hex}$-SP) shows a reduction in the difference from the glacial maxima toward the interglacials. This argues for an intensified southern-sourced water mass injection into the equatorial subthermocline. Further support comes from Southern Ocean records that showed a dramatic change in $\delta^{13}C_{C.wuellerstorfi}$ at 18 ka (Bostock et al., 2004; Pahnke & Zahn, 2005). This change is also present in MD06 (Ronge et al., 2015) although not that prominent due to the lower resolution of the core. Nevertheless, these data indicate a substantial change in the depth and possibly formation of SOIW during the deglaciation with a deeper and more southward formed SOIW. At the same time at roughly 18 ka, the reestablishment of deep EUC waters with a mainly southern-sourced water mass occurred (Loubere et al., 2003, 2007). A $\delta^{13}C$ study on thermocline-dwelling *Neogloboquadrina dutertrei* demonstrates that the onset of deglacial $\delta^{13}C$ minima events in the EEP occur simultaneously with the initiation of Southern Ocean warming (Spero & Lea, 2002). This is in harmony with a stable isotope study from the EEP showing an increased inflow of SOIW at the onset of the termination (Bova et al., 2015; Pena et al., 2008, 2013). The intensified SOIW ventilation expanded further north into the ETNP, where $\delta^{13}C$ records and ε_{Nd} signatures show comparable values to Southern Ocean signatures within the last deglaciation (Basak et al., 2010; Leduc et al., 2010).

A higher SOIW contribution to the EEP water masses could have affected the biological productivity in this area. Kienast et al. (2007) found high Corg values close to ODP Site 1240 that persist from the LGM until the deglaciation when GNPIW decreases. We speculate that the high values might be explained by the simultaneous influence of both SOIW and GNPIW on productivity during the deglaciation. Furthermore, a nitrogen isotope study by Robinson et al. (2009) claims reduced nutrient consumption during the deglaciation at ODP Site 1240. However, the authors suggest that this may be the result of variable oxygen concentrations and hence water column denitrification in EEP waters during the deglaciation (Robinson et al., 2009). At the same time, an organic biomarker analysis of ODP Site 1240 proposes changes in the nutrient supply within the deglaciation (Calvo et al., 2011). The authors compared the proxies for coccolithophorid and diatom productivity with $\delta^{13}C_{N.dutertrei}$ records of ODP Site 1240 (Pena et al., 2008) and opal fluxes derived from the Southern Ocean (Anderson et al., 2009) and concluded that the changing equatorial productivity is accompanied with an increasing influence by SOIW (Calvo et al., 2011). Max et al. (2017) combined the various proxies from the EEP and argued that substantial changes in all proxies relate to an overall change in the water mass composition rather than local phenomena at the equator during the deglaciation. Therefore, we conclude that during deglaciation and interglacial times, southern-sourced water masses became relatively more dominant in the equatorial Pacific. As a consequence, the equatorial Pacific subthermocline water masses became relatively depleted in nutrients with biological productivity that further declined to modern-like conditions.

6. Conclusions

This study investigates the varying glacial/interglacial influence of extratropical intermediate waters on EEP subthermocline during the past 240 ka. The carbon isotope comparisons indicate decreasing $\Delta\delta^{13}C$ ratios between the equatorial subthermocline and the Southern Ocean intermediate depth records during peak glacials, which imply a diminishing relative contribution from SOIW (Figure **5**). On the other hand, the $\delta^{13}C$ comparison between EEP subthermocline record and sediment cores within the pathway of GNPIW indicate major similarities during peak glacials and argues for an enhanced GNPIW ventilation during late MIS 2 and late MIS 6 (Figure **5**). We follow the interpretation of Max et al. (2017) of a "North Pacific Nutrient Leakage" during the glacial and postulate that the leakage from northern-sourced waters on equatorial subthermocline waters was also active during the penultimate glacial period.

An increasing GNPIW influence on the equatorial subthermocline could have large effects on biological productivity, as NPIW is nutrient elevated compared to SOIW today. Given that the modern EEP acts as one of the biggest CO_2 source regions on Earth today, past changes in the biological pump of the equatorial Pacific might have affected the balance between oceanic and atmospheric CO_2 concentrations. There is growing debate whether the EEP turned into a sink for atmospheric CO_2 during at least the last glacial (Martínez-Botí et al., 2015; Sanyal & Bijma, 1999). The repeated expansion of nutrient-rich GNPIW as

postulated by the "North Pacific Nutrient Leakage" might be another piece of the puzzle to further understand atmospheric CO_2 variations during the Pleistocene and in particular during peak glacial periods.

Acknowledgments
This research used samples provided by the Ocean Drilling Program (ODP). ODP is sponsored by the U.S. National Science Foundation (NSF) and participating countries under the management of Joint Oceanographic Institutions (JOI), Inc. We are grateful to L. Schönborn and G. Meyer for conducting stable isotope measurements at the AWI stable isotope lab. N.R. was funded by the German Ministry for Education and Research (BMBF—Bundesministerium für Bildung und Forschung) in the framework of the joint project Manihiki II (03G0225B). L.M. received funding through the Helmholtz Climate Initiative REKLIM (Regional climate change). The data of this study are available at PANGEA (URL: http://www.pangaea.de; https://doi.pangaea.de/10.1594/PANGAEA.882520).

References

Anderson, R. F., Ali, S., Bradtmiller, L. I., Nielsen, S. H. H., Fleisher, M. Q., Anderson, B. E., & Burckle, L. H. (2009). Wind-driven upwelling in the Southern Ocean and the deglacial rise in atmospheric CO_2. *Science*, *323*(5920), 1443–1448. https://doi.org/10.1126/science.1167441

Basak, C., Martin, E. E., Horikawa, K., & Marchitto, T. M. (2010). Southern Ocean source of ^{14}C-depleted carbon in the North Pacific Ocean during the last deglaciation. *Nature Geoscience*, *3*(11), 770–773. https://doi.org/10.1038/ngeo987

Berger, W. H., Killingley, J. S., & Vincent, E. (1978). Stable isotopes in deep-sea carbonates – Box core Erdc-92, West Equatorial Pacific. *Oceanologica Acta*, *1*, 203–216.

Beucher, C. P., Brzezinski, M. A., & Crosta, X. (2007). Silicic acid dynamics in the glacial sub-Antarctic: Implications for the silicic acid leakage hypothesis. *Global Biogeochemical Cycles*, *21*, GB3015. https://doi.org/10.1029/2006GB002746

Birch, H., Coxall, H. K., Pearson, P. N., Kroon, D., & O'Regan, M. (2013). Planktonic foraminifera stable isotopes and water column structure: Disentangling ecological signals. *Marine Micropaleontology*, *101*, 127–145. https://doi.org/10.1016/j.marmicro.2013.02.002

Bostock, H. C., Opdyke, B. N., & Williams, M. J. M. (2010). Characterising the intermediate depth waters of the Pacific Ocean using $\delta^{13}C$ and other geochemical tracers. *Deep Sea Research Part I: Oceanographic Research Papers*, *57*(7), 847–859. https://doi.org/10.1016/j.dsr.2010.04.005

Bostock, H. C., Opdyke, B. N., Gagan, M. K., & Fifield, L. K. (2004). Carbon isotope evidence for changes in Antarctic Intermediate Water circulation and ocean ventilation in the southwest Pacific during the last deglaciation. *Paleoceanography*, *19*, PA4013. https://doi.org/10.1029/2004PA001047

Bostock, H. C., Sutton, P. J., Williams, M. J. M., & Opdyke, B. N. (2013). Reviewing the circulation and mixing of Antarctic Intermediate Water in the South Pacific using evidence from geochemical tracers and Argo float trajectories. *Deep Sea Research Part I: Oceanographic Research Papers*, *73*, 84–98. https://doi.org/10.1016/j.dsr.2012.11.007

Bova, S. C., Herbert, T., Rosenthal, Y., Kalansky, J., Altabet, M., Chazen, C., … Zech, J. (2015). Links between eastern equatorial Pacific stratification and atmospheric CO_2 rise during the last deglaciation. *Paleoceanography*, *30*, 1407–1424. https://doi.org/10.1002/2015PA002816

Bradtmiller, L. I., Anderson, R. F., Fleisher, M. Q., & Burckle, L. H. (2009). Comparing glacial and Holocene opal fluxes in the Pacific sector of the Southern Ocean. *Paleoceanography*, *24*, PA2214. https://doi.org/10.1029/2008PA001693

Broecker, W. S., & Maier-Reimer, E. (1992). The influence of air and sea exchange on the carbon isotope distribution in the sea. *Global Biogeochemical Cycles*, *6*(3), 315–320. https://doi.org/10.1029/92GB01672

Broecker, W. S., & Peng, T. H. (1982). *Tracers in the sea* (p. 702). Palisades, New York: Lamont-Doherty Geological Observatory, Columbia University.

Brunelle, B. G., Sigman, D. M., Jaccard, S. L., Keigwin, L. D., Plessen, B., Schettler, G., … Haug, G. H. (2010). Glacial/interglacial changes in nutrient supply and stratification in the western subarctic North Pacific since the penultimate glacial maximum. *Quaternary Science Reviews*, *29*(19-20), 2579–2590. https://doi.org/10.1016/j.quascirev.2010.03.010

Brzezinski, M. A., Pride, C. J., Franck, V. M., Sigman, D. M., Sarmiento, J. L., Matsumoto, K., … Coale, K. H. (2002). A switch from $Si(OH)_4$ to NO_3^- depletion in the glacial Southern Ocean. *Geophysical Research Letters*, *29*(12), 5164. https://doi.org/10.1029/2001GL014349

Calvo, E., Pelejero, C., Pena, L. D., Cacho, I., & Logan, G. A. (2011). Eastern equatorial Pacific productivity and related-CO_2 changes since the last glacial period. *Proceedings of the National Academy of Sciences of the United States of America*, *108*(14), 5537–5541. https://doi.org/10.1073/pnas.1009761108

Carriquiry, J. D., Sanchez, A., & Leduc, G. (2015). Southern Ocean influence on the eastern tropical North Pacific's intermediate-depth circulation during the Last Glacial Maximum. *Paleoceanography*, *30*, 1132–1151. https://doi.org/10.1002/2014PA002766

Charles, C. D., & Fairbanks, R. G. (1992). Evidence from Southern Ocean sediments for the effect of North Atlantic deep-water flux on climate. *Nature*, *355*, 416–419. https://doi.org/10.1038/355416a0

Coale, K. H., Johnson, K. S., Fitzwater, S. E., Blain, S. P. G., Stanton, T. P., & Coley, T. L. (1998). IronEx-I, an in situ iron-enrichment experiment: Experimental design, implementation and results. *Deep Sea Research Part II: Topical Studies in Oceanography*, *45*(6), 919–945. https://doi.org/10.1016/S0967-0645(98)00019-8

Colleoni, F., Wekerle, C., Näslund, J.-O., Brandefelt, J., & Masina, S. (2016). Constraint on the penultimate glacial maximum Northern Hemisphere ice topography (≈140 kyrs BP). *Quaternary Science Reviews*, *137*, 97–112. https://doi.org/10.1016/j.quascirev.2016.01.024

Cravatte, S., Kessler, W. S., & Marin, F. (2012). Intermediate Zonal Jets in the Tropical Pacific Ocean Observed by Argo Floats. *Journal of Physical Oceanography*, *42*, 1475–1485. https://doi.org/10.1175/JPO-D-11-0206.1

Curry, W. B., & Oppo, D. W. (2005). Glacial water mass geometry and the distribution of $\delta^{13}C$ of ΣCO_2 in the western Atlantic Ocean. *Paleoceanography*, *20*, PA1017. https://doi.org/10.1029/2004PA001021

de la Fuente, M., Skinner, L., Calvo, E., Pelejero, C., & Cacho, I. (2015). Increased reservoir ages and poorly ventilated deep waters inferred in the glacial eastern equatorial Pacific. *Nature Communications*, *6*(7420), 7420. https://doi.org/10.1038/ncomms8420

Dubois, N., & Kienast, M. (2011). Spatial reorganization in the equatorial divergence in the eastern tropical Pacific during the last 150 kyr. *Geophysical Research Letters*, *38*, L16606. https://doi.org/10.1029/2011GL048325

Dugdale, R. C., Lyle, M., Wilkerson, F. P., Chai, F., Barber, R. T., & Peng, T. H. (2004). Influence of equatorial diatom processes on Si deposition and atmospheric CO_2 cycles at glacial/interglacial timescales. *Paleoceanography*, *19*, PA3011. https://doi.org/10.1029/2003PA000929

Dugdale, R. C., & Wilkerson, F. P. (1998). Silicate regulation of new production in the equatorial Pacific upwelling. *Nature*, *391*(6664), 270–273. https://doi.org/10.1038/34630

Dugdale, R. C., Wischmeyer, A. G., Wilkerson, F. P., Barber, R. T., Chai, F., Jiang, M. S., & Peng, T. H. (2002). Meridional asymmetry of source nutrients to the equatorial Pacific upwelling ecosystem and its potential impact on ocean–atmosphere CO_2 flux; A data and modeling approach. *Deep Sea Research Part II: Topical Studies in Oceanography*, *49*(13-14), 2513–2531. https://doi.org/10.1016/S0967-0645(02)00046-2

Duplessy, J. C., Shackleton, N. J., Fairbanks, R. G., Labeyrie, L., Oppo, D., & Kallel, N. (1988). Deepwater source variations during the last climatic cycle and their impact on the global deepwater circulation. *Paleoceanography*, *3*(3), 343–360. https://doi.org/10.1029/PA003i003p00343

Duplessy, J.-C., Shackleton, N. J., Matthews, R. K., Prell, W., Ruddiman, W. F., Caralp, M., & Hendy, C. H. (1984). ^{13}C record of benthic foraminifera in the last interglacial ocean: Implications for the carbon cycle and the global deep water circulation. *Quaternary Research*, *21*(02), 225–243. https://doi.org/10.1016/0033-5894(84)90099-1

Elmore, A. C., McClymont, E. L., Elderfield, H., Kender, S., Cook, M. R., Leng, M. J., … Misra, S. (2015). Antarctic intermediate water properties since 400 ka recorded in infaunal (*Uvigerina peregrina*) and epifaunal (*Planulina wuellerstorfi*) benthic foraminifera. *Earth and Planetary Science Letters*, *428*, 193–203. https://doi.org/10.1016/j.epsl.2015.07.013

Fiedler, P. C., & Talley, L. D. (2006). Hydrography of the eastern tropical Pacific: A review. *Progress in Oceanography*, *69*(2-4), 143–180. https://doi.org/10.1016/j.pocean.2006.03.008

Fine, R. A., Lukas, R., Bingham, F. M., Warner, M. J., & Gammon, R. H. (1994). The western equatorial Pacific: A water mass crossroads. *Journal of Geophysical Research*, *99*(C12), 25,063–25,080. https://doi.org/10.1029/94JC02277

Firing, E., Wijffels, S. E., & Hacker, P. (1998). Equatorial subthermocline currents across the Pacific. *Journal of Geophysical Research*, *103*(C10), 21,413–21,423. https://doi.org/10.1029/98JC01944

Galbraith, E. D., Kienast, M., Jaccard, S. L., Pedersen, T. F., Brunelle, B. G., Sigman, D. M., & Kiefer, T. (2008). Consistent relationship between global climate and surface nitrate utilization in the western subarctic Pacific throughout the last 500 ka. *Paleoceanography*, *23*, PA2212. https://doi.org/10.1029/2007PA001518

Gebbie, G., Peterson, C. D., Lisiecki, L. E., & Spero, H. J. (2015). Global-mean marine ^{13}C and its uncertainty in a glacial state estimate. *Quaternary Science Reviews*, *125*, 144–159. https://doi.org/10.1016/j.quascirev.2015.08.010

Gebhardt, H., Sarnthein, M., Grootes, P. M., Kiefer, T., Kuehn, H., Schmieder, F., & Röhl, U. (2008). Paleonutrient and productivity records from the subarctic North Pacific for Pleistocene glacial Terminations I to V. *Paleoceanography*, *23*, PA4212. https://doi.org/10.1029/2007PA001513

Goodman, P. J., Hazeleger, W., de Vries, P., & Cane, M. (2005). Pathways into the Pacific equatorial undercurrent: A trajectory analysis. *Journal of Physical Oceanography*, *35*(11), 2134–2151. https://doi.org/10.1175/JPO2825.1

Gordon, R. M., Coale, K. H., & Johnson, K. S. (1997). Iron distributions in the equatorial Pacific: Implications for new production. *Limnology and Oceanography*, *42*(3), 419–431. https://doi.org/10.4319/lo.1997.42.3.0419

Hebbeln, D., Marchant, M., & Wefer, G. (2002). Paleoproductivity in the southern Peru–Chile Current through the last 33 000 yr. *Marine Geology*, *186*(3-4), 487–504. https://doi.org/10.1016/S0025-3227(02)00331-6

Hendry, K. R., & Brzezinski, M. A. (2014). Using silicon isotopes to understand the role of the Southern Ocean in modern and ancient biogeochemistry and climate. *Quaternary Science Reviews*, *89*, 13–26. https://doi.org/10.1016/j.quascirev.2014.01.019

Herguera, J. C., Herbert, T., Kashgarian, M., & Charles, C. (2010). Intermediate and deep water mass distribution in the Pacific during the Last Glacial Maximum inferred from oxygen and carbon stable isotopes. *Quaternary Science Reviews*, *29*(9-10), 1228–1245. https://doi.org/10.1016/j.quascirev.2010.02.009

Horikawa, K., Asahara, Y., Yamamoto, K., & Okazaki, Y. (2010). Intermediate water formation in the Bering Sea during glacial periods: Evidence from neodymium isotope ratios. *Geology*, *38*(5), 435–438. https://doi.org/10.1130/g30225.1

Hu, R., Piotrowski, A. M., Bostock, H. C., Crowhurst, S., & Rennie, V. (2016). Variability of neodymium isotopes associated with planktonic foraminifera in the Pacific Ocean during the Holocene and Last Glacial Maximum. *Earth and Planetary Science Letters*, *447*, 130–138. https://doi.org/10.1016/j.epsl.2016.05.011

Huang, K.-F., Oppo, D. W., & Curry, W. B. (2014). Decreased influence of Antarctic intermediate water in the tropical Atlantic during North Atlantic cold events. *Earth and Planetary Science Letters*, *389*, 200–208. https://doi.org/10.1016/j.epsl.2013.12.037

Jaccard, S. L., Haug, G. H., Sigman, D. M., Pedersen, T. F., Thierstein, H. R., & Röhl, U. (2005). Glacial/interglacial changes in subarctic North Pacific stratification. *Science*, *308*(5724), 1003–1006. https://doi.org/10.1126/science.1108696

Keigwin, L. D. (1998). Glacial-age hydrography of the far northwest Pacific Ocean. *Paleoceanography*, *13*(4), 323–339. https://doi.org/10.1029/98PA00874

Kessler, W. S. (2006). The circulation of the eastern tropical Pacific: A review. *Progress in Oceanography*, *69*(2-4), 181–217. https://doi.org/10.1016/j.pocean.2006.03.009

Key, R. M., Kozyr, A., Sabine, C. L., Lee, K., Wanninkhof, R., Bullister, J. L., … Peng, T.-H. (2004). A global ocean carbon climatology: Results from Global Data Analysis Project (GLODAP). *Global Biogeochemical Cycles*, *18*, GB4031. https://doi.org/10.1029/2004GB002247

Kienast, S. S., Hendy, I. L., Crusius, J., Pedersen, T. F., & Calvert, S. E. (2004). Export production in the subarctic North Pacific over the last 800 kyrs: No evidence for iron fertilization? *Journal of Oceanography*, *60*(1), 189–203. https://doi.org/10.1023/B:JOCE.0000038326.73943.aa

Kienast, S. S., Kienast, M., Mix, A. C., Calvert, S. E., & François, R. (2007). Thorium-230 normalized particle flux and sediment focusing in the Panama Basin region during the last 30,000 years. *Paleoceanography*, *22*, PA2213. https://doi.org/10.1029/2006PA001357

Kim, S., Khim, B. K., Uchida, M., Itaki, T., & Tada, R. (2011). Millennial-scale paleoceanographic events and implication for the intermediate-water ventilation in the northern slope area of the Bering Sea during the last 71 kyrs. *Global and Planetary Change*, *79*(1-2), 89–98. https://doi.org/10.1016/j.gloplacha.2011.08.004

Knudson, K. P., & Ravelo, A. C. (2015a). Enhanced subarctic Pacific stratification and nutrient utilization during glacials over the last 1.2 Myr. *Geophysical Research Letters*, *42*, 9870–9879. https://doi.org/10.1002/2015GL066317

Knudson, K. P., & Ravelo, A. C. (2015b). North Pacific Intermediate Water circulation enhanced by the closure of the Bering Strait. *Paleoceanography*, *30*, 1287–1304. https://doi.org/10.1002/2015PA002840

Kroopnick, P. M. (1985). The distribution of ^{13}C of ΣCO_2 in the world oceans. *Deep Sea Research Part A. Oceanographic Research Papers*, *32*(1), 57–84. https://doi.org/10.1016/0198-0149(85)90017-2

Kuehn, H., Lembke-Jene, L., Gersonde, R., Esper, O., Lamy, F., Arz, H., … Tiedemann, R. (2014). Laminated sediments in the Bering Sea reveal atmospheric teleconnections to Greenland climate on millennial to decadal timescales during the last deglaciation. *Climate of the Past*, *10*(6), 2215–2236. https://doi.org/10.5194/cp-10-2215-2014

Le Borgne, R., Feely, R. A., & Mackey, D. J. (2002). Carbon fluxes in the equatorial Pacific: A synthesis of the JGOFS programme. *Deep Sea Research Part II: Topical Studies in Oceanography*, *49*(13-14), 2425–2442. https://doi.org/10.1016/S0967-0645(02)00043-7

Leduc, G., Vidal, L., Tachikawa, K., & Bard, E. (2010). Changes in eastern Pacific Ocean ventilation at intermediate depth over the last 150 kyr BP. *Earth and Planetary Science Letters*, *298*(1-2), 217–228. https://doi.org/10.1016/j.epsl.2010.08.002

Lisiecki, L. E. (2010). A simple mixing explanation for late Pleistocene changes in the Pacific-South Atlantic benthic $\delta^{13}C$ gradient. *Climate of the Past*, *6*(3), 305–314. https://doi.org/10.5194/cp-6-305-2010

Lisiecki, L. E., & Raymo, M. E. (2005). A Pliocene–Pleistocene stack of 57 globally distributed benthic $\delta^{18}O$ records. *Paleoceanography*, *20*, PA1003. https://doi.org/10.1029/2004PA001071

Locarnini, R. A., Mishonov, A. V., Antonov, J. I., Boyer, T. P., Garcia, H. E., Baranova, O. K., … Seidov, D. (2013). World ocean atlas 2013, volume 1: Temperature. In S. Levitus & A. Mishonov (Eds.), *NOAA atlas NESDIS 73* (p. 40). MD: NOAA, Silver Spring.

Loubere, P., Fariduddin, M., & Murray, R. W. (2003). Patterns of export production in the eastern equatorial Pacific over the past 130,000 years. *Paleoceanography*, *18*, 1028. https://doi.org/10.1029/2001PA000658

Loubere, P., Fariduddin, M., & Richaud, M. (2011). Glacial marine nutrient and carbon redistribution: Evidence from the tropical ocean. *Geochemistry, Geophysics, Geosystems*, *12*, Q08013. https://doi.org/10.1029/2011GC003546

Loubere, P., Richaud, M., & Mireles, S. (2007). Variability in tropical thermocline nutrient chemistry on the glacial/interglacial timescale. *Deep Sea Research Part II: Topical Studies in Oceanography*, *54*(5-7), 747–761. https://doi.org/10.1016/j.dsr2.2007.01.005

Lund, D. C., & Mix, A. C. (1998). Millennial-scale deep water oscillations: Reflections of the North Atlantic in the deep Pacific from 10 to 60 ka. *Paleoceanography*, *13*(1), 10–19. https://doi.org/10.1029/97PA02984

Lutze, G., & Thiel, H. (1989). Epibenthic foraminifera from elevated microhabitats: *Cibicidoides wuellerstorfi* and *Planulina ariminensis*. *Journal of Foraminiferal Research*, *19*(2), 153–158. https://doi.org/10.2113/gsjfr.19.2.153

Mackensen, A. (2012). Strong thermodynamic imprint on recent bottom-water and epibenthic $\delta^{13}C$ in the Weddell Sea revealed: Implications for glacial Southern Ocean ventilation. *Earth and Planetary Science Letters*, *317-318*, 20–26. https://doi.org/10.1016/j.epsl.2011.11.030

Mackensen, A., Hubberten, H. W., Bickert, T., Fischer, G., & Fütterer, D. K. (1993). The $\delta^{13}C$ in benthic foraminiferal tests of *Fontbotia wuellerstorfi* (Schwager) relative to the $\delta^{13}C$ of dissolved inorganic carbon in Southern Ocean deep water: Implications for glacial ocean circulation models. *Paleoceanography*, *8*(5), 587–610. https://doi.org/10.1029/93PA01291

Mackey, D. J., O'Sullivan, J. E., & Watson, R. J. (2002). Iron in the western Pacific: A riverine or hydrothermal source for iron in the equatorial undercurrent? *Deep Sea Research Part I: Oceanographic Research Papers*, *49*(5), 877–893. https://doi.org/10.1016/S0967-0637(01)00075-9

Martin, J. H., Coale, K. H., Johnson, K. S., Fitzwater, S. E., Gordon, R. M., Tanner, S. J., … Tindale, N. W. (1994). Testing the iron hypothesis in ecosystems of the equatorial Pacific Ocean. *Nature*, *371*(6493), 123–129. https://doi.org/10.1038/371123a0

Martínez-Botí, M. A., Marino, G., Foster, G. L., Ziveri, P., Henehan, M. J., Rae, J. W. B., … Vance, D. (2015). Boron isotope evidence for oceanic carbon dioxide leakage during the last deglaciation. *Nature*, *518*(7538), 219–222. https://doi.org/10.1038/nature14155

Matsumoto, K., Oba, T., Lynch-Stieglitz, J., & Yamamoto, H. (2002). Interior hydrography and circulation of the glacial Pacific Ocean. *Quaternary Science Reviews*, *21*(14-15), 1693–1704. https://doi.org/10.1016/S0277-3791(01)00142-1

Matsumoto, K., Sarmiento, J. L., & Brzezinski, M. A. (2002). Silicic acid leakage from the Southern Ocean: A possible explanation for glacial atmospheric pCO_2, *Global Biogeochemical Cycles*, *16*(3), 5-1–5-23. https://doi.org/10.1029/2001GB001442

Matul, A. G., Abelmann, A., Gersonde, R., Nürnberg, D., Tiedemann, R., & Kruglikova, S. B. (2015). Late Quaternary distribution of the *Cycladophora davisiana* radiolarian species: Reflection of possible ventilation of the North Pacific Intermediate Water during the Last Glacial Maximum. *Oceanology*, *55*(1), 91–99. https://doi.org/10.1134/s0001437015010130

Max, L., Belz, L., Tiedemann, R., Fahl, K., Nürnberg, D., & Riethdorf, J.-R. (2014). Rapid shifts in subarctic Pacific climate between 138 and 70 ka. *Geology*, *42*(10), 899–902. https://doi.org/10.1130/g35879.1

Max, L., Lembke-Jene, L., Riethdorf, J. R., Tiedemann, R., Nürnberg, D., Kühn, H., & Mackensen, A. (2014). Pulses of enhanced North Pacific Intermediate Water ventilation from the Okhotsk Sea and Bering Sea during the last deglaciation. *Climate of the Past*, *10*(2), 591–605. https://doi.org/10.5194/cp-10-591-2014

Max, L., Rippert, N., Lembke-Jene, L., Mackensen, A., Nürnberg, D., & Tiedemann, R. (2017). Evidence for enhanced convection of North Pacific Intermediate Water to the low-latitude Pacific under glacial conditions. *Paleoceanography*, *32*, 41–55. https://doi.org/10.1002/2016PA002994

McCartney, M. S. (1977). Subantarctic mode water. In M. V. Angel (Ed.), *A voyage of discovery: George Deacon 70th anniversary volume* (pp. 103–119). Pergamon Press, Oxford.

McCave, I. N., Carter, L., & Hall, I. R. (2008). Glacial–interglacial changes in water mass structure and flow in the SW Pacific Ocean. *Quaternary Science Reviews*, *27*(19-20), 1886–1908. https://doi.org/10.1016/j.quascirev.2008.07.010

McCreary, J. P., & Lu, P. (2001). Influence of the Indonesian Throughflow on the circulation of intermediate water in the Pacific Ocean. *Journal of Physical Oceanography*, *31*, 932–942.

Menviel, L., Yu, J., Joos, F., Mouchet, A., Meissner, K. J., & England, M. H. (2016). Poorly ventilated deep ocean at the Last Glacial Maximum inferred from carbon isotopes: A data–model comparison study. *Paleoceanography*, *32*, 2–17. https://doi.org/10.1002/2016PA003024

Mix, A. C., Pisias, N. G., Rugh, W., Wilson, J., Morey, A., & Hagelberg, T. K. (1995). Benthic foraminifers stable isotope record from Site 849 (0–5 Ma): Local and global climate change. *Proceeding of the Ocean Drilling Program, Scientific Results*, *138*, 371–412.

Mix, A. C., Pisias, N. G., Zahn, R., Rugh, W., Lopez, C., & Nelson, K. (1991). Carbon 13 in Pacific deep and intermediate waters, 0–370 ka: Implications for ocean circulation and Pleistocene CO_2. *Paleoceanography*, *6*(2), 205–226. https://doi.org/10.1029/90PA02303

Mix, A. C., Tiedemann, R., & Blum, P. (2003). *Shipboard scientific party. Leg 202 summary* (pp. 1–145). College Station, TX: Ocean Drilling Program. https://doi.org/10.2973/odp.proc.ir.202.2003

Monnin, E., Indermühle, A., Dällenbach, A., Flückiger, J., Stauffer, B., Stocker, T. F., … Barnola, J.-M. (2001). Atmospheric CO_2 concentrations over the last glacial termination. *Science*, *291*(5501), 112–114. https://doi.org/10.1126/science.291.5501.112

Muratli, J. M., Chase, Z., Mix, A. C., & McManus, J. (2010). Increased glacial-age ventilation of the Chilean margin by Antarctic Intermediate Water. *Nature Geoscience*, *3*(1), 23–26. https://doi.org/10.1038/ngeo715

Ninkovich, D., & Shackleton, N. J. (1975). Distribution, stratigraphic position and age of ash layer "L", in the Panama Basin region. *Earth and Planetary Science Letters*, *27*(1), 20–34. https://doi.org/10.1016/0012-821X(75)90156-9

Nürnberg, D., Dethleff, D., Tiedemann, R., Kaiser, A., & Gorbarenko, S. A. (2011). Okhotsk Sea ice coverage and Kamchatka glaciation over the last 350 ka—Evidence from ice-rafted debris and planktonic $\delta^{18}O$. *Palaeogeography, Palaeoclimatology, Palaeoecology*, *310*(3-4), 191–205. https://doi.org/10.1016/j.palaeo.2011.07.011

Oppo, D. W., & Fairbanks, R. G. (1989). Carbon isotope composition of tropical surface water during the past 22,000 years. *Paleoceanography*, *4*(4), 333–351. https://doi.org/10.1029/PA004i004p00333

Oppo, D. W., & Fairbanks, R. G. (1990). Atlantic Ocean thermohaline circulation of the last 150,000 years: Relationship to climate and atmospheric CO_2. *Paleoceanography*, *5*(3), 277–288. https://doi.org/10.1029/PA005i003p00277

Ortiz, J. D., Mix, A. C., Rugh, W., Watkins, J. M., & Collier, R. W. (1996). Deep-dwelling planktonic foraminifera of the northeastern Pacific Ocean reveal environmental control of oxygen and carbon isotopic disequilibria. *Geochimica et Cosmochimica Acta*, *60*(22), 4509–4523. https://doi.org/10.1016/S0016-7037(96)00256-6

Pahnke, K., Goldstein, S. L., & Hemming, S. R. (2008). Abrupt changes in Antarctic Intermediate Water circulation over the past 25,000 years. *Nature Geoscience*, *1*(12), 870–874. https://doi.org/10.1038/ngeo360

Pahnke, K., Sachs, J. P., Keigwin, L., Timmermann, A., & Xie, S.-P. (2007). Eastern tropical Pacific hydrologic changes during the past 27,000 years from D/H ratios in alkenones. *Paleoceanography*, *22*, PA4214. https://doi.org/10.1029/2007PA001468

Pahnke, K., & Zahn, R. (2005). Southern Hemisphere water mass conversion linked with North Atlantic climate variability. *Science*, *307*(5716), 1741–1746. https://doi.org/10.1126/science.1102163

Paillard, D., Labeyrie, L., & Yiou, P. (1996). Macintosh program performs time-series analysis. *Eos, Transactions of the American Geophysical Union*, *77*(39), 379–379. https://doi.org/10.1029/96EO00259

Pena, L. D., Cacho, I., Ferretti, P., & Hall, M. A. (2008). El Niño–Southern Oscillation-like variability during glacial terminations and interlatitudinal teleconnections. *Paleoceanography*, *23*, PA3101. https://doi.org/10.1029/2008PA001620

Pena, L. D., Goldstein, S. L., Hemming, S. R., Jones, K. M., Calvo, E., Pelejero, C., & Cacho, I. (2013). Rapid changes in meridional advection of Southern Ocean intermediate waters to the tropical Pacific during the last 30 kyr. *Earth and Planetary Science Letters*, *368*, 20–32. https://doi.org/10.1016/j.epsl.2013.02.028

Pépin, L., Raynaud, D., Barnola, J.-M., & Loutre, M. F. (2001). Hemispheric roles of climate forcings during glacial–interglacial transitions as deduced from the Vostok record and LLN-2D model experiments. *Journal of Geophysical Research*, *106*(D23), 31,885–31,892. https://doi.org/10.1029/2001JD900117

Peterson, C. D., Lisiecki, L. E., & Stern, J. V. (2014). Deglacial whole-ocean $\delta^{13}C$ change estimated from 480 benthic foraminiferal records. *Paleoceanography*, *29*, 549–563. https://doi.org/10.1002/2013PA002552

Petit, J. R., Jouzel, J., Raynaud, D., Barkov, N. I., Barnola, J. M., Basile, I., … Stievenard, M. (1999). Climate and atmospheric history of the past 420,000 years from the Vostok ice core, Antarctica. *Nature*, *399*(6735), 429–436. https://doi.org/10.1038/20859

Pichevin, L. E., Reynolds, B. C., Ganeshram, R. S., Cacho, I., Pena, L., Keefe, K., & Ellam, R. M. (2009). Enhanced carbon pump inferred from relaxation of nutrient limitation in the glacial ocean. *Nature*, *459*(7250), 1114–1117. https://doi.org/10.1038/nature08101

Qu, T., Gao, S., Fukumori, I., Fine, R. A., & Lindstrom, E. J. (2009). Origin and pathway of equatorial 13°C water in the Pacific identified by a simulated passive tracer and its adjoint. *Journal of Physical Oceanography*, *39*(8), 1836–1853. https://doi.org/10.1175/2009JPO4045.1

Qu, T., & Lindstrom, E. J. (2004). Northward intrusion of Antarctic Intermediate Water in the western Pacific. *Journal of Physical Oceanography*, *34*(9), 2104–2118. https://doi.org/10.1175/1520-0485(2004)034%3C2104:NIOAIW%3E2.0.CO;2

Rafter, P. A., & Sigman, D. M. (2015). Spatial distribution and temporal variation of nitrate nitrogen and oxygen isotopes in the upper equatorial Pacific Ocean. *Limnology and Oceanography*, *61*(1), 14–31. https://doi.org/10.1002/lno.10152

Raynaud, D., Barnola, J.-M., Souchez, R., Lorrain, R., Petit, J.-R., Duval, P., & Lipenkov, V. Y. (2005). Palaeoclimatology: The record for marine isotopic stage 11. *Nature*, *436*(7047), 39–40. https://doi.org/10.1038/43639b

Reid, J. L. (1965). *Intermediate water of the Pacific Ocean*, *Johns Hopkins oceanographic studies no. 2* (p. 85). Baltimore, MD: John Hopkins Press.

Rella, S. F., Tada, R., Nagashima, K., Ikehara, M., Itaki, T., Ohkushi, K. I., … Uchida, M. (2012). Abrupt changes of intermediate water properties on the northeastern slope of the Bering Sea during the last glacial and deglacial period. *Paleoceanography*, *27*, PA3203. https://doi.org/10.1029/2011PA002205

Rickaby, R. E. M., & Elderfield, H. (2005). Evidence from the high-latitude North Atlantic for variations in Antarctic Intermediate Water flow during the last deglaciation. *Geochemistry, Geophysics, Geosystems*, *6*, Q05001. https://doi.org/10.1029/2004GC000858

Riethdorf, J.-R., Thibodeau, B., Ikehara, M., Nürnberg, D., Max, L., Tiedemann, R., & Yokoyama, Y. (2016). Surface nitrate utilization in the Bering sea since 180 kA BP: Insight from sedimentary nitrogen isotopes. *Deep Sea Research Part II: Topical Studies in Oceanography*, *125-126*, 163–176. https://doi.org/10.1016/j.dsr2.2015.03.007

Rippert, N., Nürnberg, D., Raddatz, J., Maier, E., Hathorne, E., Bijma, J., & Tiedemann, R. (2016). Constraining foraminiferal calcification depths in the western Pacific warm pool. *Marine Micropaleontology*, *128*, 14–27. https://doi.org/10.1016/j.marmicro.2016.08.004

Robinson, R. S., Brzezinski, M. A., Beucher, C. P., Horn, M. G. S., & Bedsole, P. (2014). The changing roles of iron and vertical mixing in regulating nitrogen and silicon cycling in the Southern Ocean over the last glacial cycle. *Paleoceanography*, *29*, 1179–1195. https://doi.org/10.1002/2014PA002686

Robinson, R. S., Martinez, P., Pena, L. D., & Cacho, I. (2009). Nitrogen isotopic evidence for deglacial changes in nutrient supply in the eastern equatorial Pacific. *Paleoceanography*, *24*, PA4213. https://doi.org/10.1029/2008PA001702

Rohling, E. J., & Cook, S. (1999). Stable oxygen and carbon isotope ratios in foraminiferal carbonate. In B. K. Sen Gupta (Ed.), *Modern foraminifera* (pp. 239–258). Dordrecht, Netherlands: Kluwer Academic. https://doi.org/10.1007/0-306-48104-9_14

Ronge, T. A., Steph, S., Tiedemann, R., Prange, M., Merkel, U., Nürnberg, D., & Kuhn, G. (2015). Pushing the boundaries: Glacial/interglacial variability of intermediate and deep waters in the southwest Pacific over the last 350,000 years. *Paleoceanography*, *30*, 23–38. https://doi.org/10.1002/2014PA002727

Ronge, T. A., Tiedemann, R., Lamy, F., Köhler, P., Alloway, B. V., De Pol-Holz, R., … Wacker, L. (2016). Radiocarbon constraints on the extent and evolution of the South Pacific glacial carbon pool. *Nature Communication*, *7*. https://doi.org/10.1038/ncomms11487

Rousseau, J., Ellwood, M. J., Bostock, H., & Neil, H. (2016). Estimates of late Quaternary mode and intermediate water silicic acid concentration in the Pacific Southern Ocean. *Earth and Planetary Science Letters*, *439*, 101–108. https://doi.org/10.1016/j.epsl.2016.01.023

Ryan, J. P., Ueki, I., Chao, Y., Zhang, H., Polito, P. S., & Chavez, F. P. (2006). Western Pacific modulation of large phytoplankton blooms in the central and eastern equatorial Pacific. *Journal of Geophysical Research*, *111*, G02013. https://doi.org/10.1029/2005JG000084

Sanyal, A., & Bijma, J. (1999). A comparative study of the northwest Africa and eastern equatorial Pacific upwelling zones as sources of CO_2 during glacial periods based on boron isotope paleo-pH estimation. *Paleoceanography*, *14*(6), 753–759. https://doi.org/10.1029/1999PA900036

Sarmiento, J. L., Gruber, N., Brzezinski, M. A., & Dunne, J. P. (2004). High-latitude controls of thermocline nutrients and low latitude biological productivity. *Nature*, *427*(6969), 56–60. https://doi.org/10.1038/nature02127

Schlitzer, R. (2015). Ocean data view. Retrieved from http://odv.awi.de

Schlung, S. A., Christina Ravelo, A., Aiello, I. W., Andreasen, D. H., Cook, M. S., Drake, M., … Takahashi, K. (2013). Millennial-scale climate change and intermediate water circulation in the Bering Sea from 90 ka: A high-resolution record from IODP Site U1340. *Paleoceanography*, *28*, 54–67. https://doi.org/10.1029/2012PA002365

Schmittner, A., Gruber, N., Mix, A. C., Key, R. M., Tagliabue, A., & Westberry, T. K. (2013). Biology and air-sea gas exchange controls on the distribution of carbon isotope ratios ($\delta^{13}C$) in the ocean. *Biogeosciences*, *10*(9), 5793–5816. https://doi.org/10.5194/bg-10-5793-2013

Shaari, H. b., Yamamoto, M., & Irino, T. (2013). Enhanced upwelling in the eastern equatorial Pacific at the last five glacial terminations. *Palaeogeography, Palaeoclimatology, Palaeoecology*, *386*, 8–15. https://doi.org/10.1016/j.palaeo.2013.03.022

Shackleton, N. J., & Opdyke, N. D. (1973). Oxygen isotope and palaeomagnetic stratigraphy of equatorial Pacific core V28-238: Oxygen isotope temperatures and ice volumes on a 105 year and 106 year scale. *Quaternary Research*, *3*(01), 39–55. https://doi.org/10.5194/bg-10-5793-2013

Shcherbina, A. Y., Talley, L. D., & Rudnick, D. L. (2003). Direct observations of North Pacific ventilation: Brine rejection in the Okhotsk Sea. *Science*, *302*(5652), 1952–1955. https://doi.org/10.1126/science.1088692

Skinner, L., McCave, I. N., Carter, L., Fallon, S., Scrivner, A. E., & Primeau, F. (2015). Reduced ventilation and enhanced magnitude of the deep Pacific carbon pool during the last glacial period. *Earth and Planetary Science Letters*, *411*, 45–52. https://doi.org/10.1016/j.epsl.2014.11.024

Skinner, L. C., Fallon, S., Waelbroeck, C., Michel, E., & Barker, S. (2010). Ventilation of the deep Southern Ocean and deglacial CO_2 rise. *Science*, *328*(5982), 1147–1151. https://doi.org/10.1126/science.1183627

Spero, H. J., & Lea, D. W. (2002). The cause of carbon isotope minimum events on glacial terminations. *Science*, *296*(5567), 522–525. https://doi.org/10.1126/science.1069401

Staines-Urías, F., González-Yajimovich, O., & Beaufort, L. (2015). Reconstruction of past climate variability and ENSO-like fluctuations in the southern Gulf of California (Alfonso Basin) since the last glacial maximum. *Quaternary Research*, *83*(03), 488–501. https://doi.org/10.1016/j.yqres.2015.03.007

Stott, L. D., Neumann, M., & Hammond, D. (2000). Intermediate water ventilation on the Northeastern Pacific Margin during the late Pleistocene inferred from benthic foraminiferal $\delta^{13}C$. *Paleoceanography*, *15*(2), 161–169. https://doi.org/10.1029/1999PA000375

Takahashi, T., Sutherland, S. C., Wanninkhof, R., Sweeney, C., Feely, R. A., Chipman, D. W., … de Baar, H. J. W. (2009). Climatological mean and decadal change in surface ocean pCO_2, and net sea–air CO_2 flux over the global oceans. *Deep Sea Research Part II: Topical Studies in Oceanography*, *56*(8-10), 554–577. https://doi.org/10.1016/j.dsr2.2008.12.009

Talley, L. D. (1993). Distribution and formation of North Pacific intermediate water. *Journal of Physical Oceanography*, *23*(3), 517–537. https://doi.org/10.1175/1520-0485(1993)023%3C0517:DAFONP%3E2.0.CO;2

Tapia, R., Nürnberg, D., Ronge, T., & Tiedemann, R. (2015). Disparities in glacial advection of Southern Ocean Intermediate Water to the South Pacific gyre. *Earth and Planetary Science Letters*, *410*, 152–164. https://doi.org/10.1016/j.epsl.2014.11.031

Tchernia, P. (1980). *Descriptive regional oceanography* (p. 253). Oxford: Pergamon Press.

Tomczak, M., & Godfrey, J. S. (2005). *Regional oceanography: An introduction* (2nd Edition 1.1 ed., p. 422). Oxford: Pergamon.

Winckler, G., Anderson, R. F., Fleisher, M. Q., McGee, D., & Mahowald, N. (2008). Covariant glacial–interglacial dust fluxes in the equatorial Pacific and Antarctica. *Science*, *320*(5872), 93–96. https://doi.org/10.1126/science.1150595

Yu, P.-S., Kienast, M., Chen, M.-T., Cacho, I., Flores, J. A., Mohtadi, M., & Mix, A. C. (2012). Influences of extratropical water masses on equatorial Pacific cold tongue variability during the past 160 ka as revealed by faunal evidence of planktic foraminifers. *Journal of Quaternary Science*, *27*(9), 921–931. https://doi.org/10.1002/jqs.2582

Zahn, R., Pedersen, T. F., Bornhold, B. D., & Mix, A. C. (1991). Water mass conversion in the glacial subarctic Pacific (54°N, 148°W): Physical constraints and the benthic–planktonic stable isotope record. *Paleoceanography*, *6*(5), 543–560. https://doi.org/10.1029/91PA01327

Zahn, R., Winn, K., & Sarnthein, M. (1986). Benthic foraminiferal $\delta^{13}C$ and accumulation rates of organic carbon: *Uvigerina peregrina* group and *Cibicidoides wuellerstorfi*. *Paleoceanography*, *1*(1), 27–42. https://doi.org/10.1029/PA001i001p00027